



# Exploring the sensitivity to precipitation, blowing snow, and horizontal resolution of the spatial distribution of simulated snow cover

Ange Haddjeri<sup>1</sup>, Matthieu Baron<sup>1</sup>, Matthieu Lafaysse<sup>1</sup>, Louis Le Toumelin<sup>1</sup>, César Deschamp-Berger<sup>2,4</sup>, Vincent Vionnet<sup>3</sup>, Simon Gascoin<sup>4</sup>, Matthieu Vernay<sup>1</sup>, and Marie Dumont<sup>1</sup>

<sup>1</sup>Univ. Grenoble Alpes, Université de Toulouse, Météo-France, CNRS, CNRM, Centre d'Études de la Neige, Grenoble, France

<sup>2</sup>Instituto Pirenaico de Ecología, Consejo Superior de Investigaciones Científicas (IPE-CSIC), Zaragoza, Spain

<sup>3</sup>Meteorological Research Division, Environment and Climate Change Canada, Dorval, QC, Canada

<sup>4</sup>Centre d'Etudes Spatiales de la Biosphère, CESBIO, Univ. Toulouse, CNES/CNRS/INRAE/IRD/UPS, Toulouse, France

**Correspondence:** ange.haddjeri@umr-cnrm.fr

**Abstract.** Accurate snow cover modeling is a high stake for mountain regions. Alpine snow evolution and spatial variability result from a multitude of complex processes including interactions between wind and snow. The SnowPappus blowing snow model was designed to add blowing snow modeling capabilities to the SURFEX/Crocus simulation system for applications across large spatial and temporal extents. This paper presents the very first spatialized evaluation of this simulation system over a 902 km<sup>2</sup> domain in the French Alps. Here we compare snow cover simulations to the spatial distribution of snow height obtained from Pleiades satellites stereo-imagery and to Snow Melt-Out Dates from Sentinel-2 time series over three snow seasons. We analyzed the sensitivity of the simulations to three different precipitation datasets and two horizontal resolutions. The evaluations are presented as a function of elevation and landform types. The results show that the SnowPappus model forced with high-resolution wind fields enhances the snow cover spatial variability at high elevations allowing a better agreement with observations above 2500 m and near peaks and ridges. Model improvements are not obvious at low to medium altitudes where precipitation errors are the prevailing uncertainty. Our study illustrates the necessity to consider error contributions from blowing snow, precipitation forcings, and unresolved subgrid variability for robust evaluations of spatialized snow simulations. Despite the significant effect of the unresolved spatial scales of snow transport, 250 m horizontal resolution snow simulations using SnowPappus are found to be a promising avenue for large-scale modeling of alpine snowpacks.

## 15 1 Introduction

Snow cover in mountainous terrains is characterized by an important variability at multiple temporal and spatial scales (Pomerooy and Gray, 1995; Clark et al., 2011; Anderson et al., 2014; Mott et al., 2018). This variability results from a large diversity of slopes, aspects, and elevations which induce a high variability of precipitation, wind, temperature, and radiation. Accurate snowpack modeling is key to describing this high variability in hydrological applications, climate projections, and hazard forecasting in mountainous terrains (IPCC, 2022; Morin et al., 2020).



The spatial variability of precipitation amount and phase at different scales is known to be one of the main sources of snowpack variability at the mountain range scale (1-100 km) (Clark et al., 2011). These patterns are specific to the regional topography and atmospheric flow, with regions of increased or decreased precipitation (Colle et al., 2013). At the slope scale (a few hundred meters), preferential deposition and snowfall enhancement are the main processes responsible for snowfall variability (before snowflake settlement) (Mott et al., 2018). The preferential deposition is the result of the interaction of the near-surface flow field with particle trajectories, creating areas of local accumulation (Lehning et al., 2008). Snowfall enhancement is a process in which surface flows are responsible for locally increased air moisture, leading to the formation or maintenance of low-level clouds, ultimately enhancing solid precipitations through a seeder-feeder mechanism (Bergeron, 1965; Choularton and Perry, 1986; Minder et al., 2011). Post-depositional processes finally, determine the snow variability at the slope scale and below. Blowing snow transport, snow sublimation, snow redistribution by avalanches, snow compaction, and melt are the main processes at work (Winstral et al., 2002; Bernhardt and Schulz, 2010; Mott et al., 2018). Blowing snow transport produces a mass transfer of snow from windward areas to leeward deposition zones. Additional mass loss occurs in those events due to the sublimation of suspended snow Liston and Sturm (1998); Yang et al. (2010). The heterogeneity of snow mass loss due to snow melt (Brauchli et al., 2017) and surface sublimation (Pomeroy et al., 1998; Strasser et al., 2008) also contribute to snowpack variability in alpine terrain.

The multi-scale variability of the alpine snowpack makes it challenging to represent in numerical models. Various approaches have been developed for that purpose. Numerical Weather Prediction (NWP) models at the kilometer scale or higher resolution models can explicitly represent the orographic precipitation patterns, and in some cases local low-level cloud formation, triggering snowfall enhancement (Lehning et al., 2006; Vionnet et al., 2017; Wang and Huang, 2017; Monteiro et al., 2022). However, the quantification of the precipitation is still impacted by important uncertainties (Clark et al., 2011; Ménard et al., 2019; Lundquist et al., 2019). Downscaling tools can be used to better represent the local meteorology from NWP models (Sen Gupta and Tarboton, 2016; Marsh et al., 2023; Bernhardt et al., 2010; Mital et al., 2022). Eventually, the representation of post-depositional processes, notably blowing snow transport, benefits from the development of dedicated high-resolution models coupled to or forced by atmospheric models (e.g., Lehning et al., 2006; Liston et al., 2007; Marsh et al., 2020; Sharma et al., 2021; Baron et al., 2023; Quéno et al., 2023).

The spatial evaluation of this last type of system is a challenge in itself. The snow modeling community has long been evaluating this kind of model locally. Evaluations can be carried out using direct measurements of the variable of interest, for example for blowing snow modeling, Vionnet et al. (2014) evaluated directly the simulated blowing snow fluxes of the Meso-NH/Crocus system against locally measured fluxes from a Snow Particle Counters (Sato et al., 1993). Amory et al. (2021) also compares simulated snow transport occurrence and mass fluxes to on-field observations in Antarctica. Similarly, Baron et al. (2023) compares the simulated snow transport occurrence and transport mass fluxes from the SnowPappus model to field observations. One of the main drawbacks of this method is the low number of direct snow transport observations found in literature, combined with the very high spatial variability of snow transport fluxes. As a result, spatialized snow simulations are more classically evaluated using measurements of snow height and Snow Water Equivalent (SWE). Prasad et al. (2001) and Liston et al. (2007) compare snow simulations done using the SnowTran-3D system (Liston and Sturm, 1998; Liston et al.,



2007) with SWE measurements from manual snow surveys. Marsh et al. (2020) compare simulated SWE from the Canadian Hydrological Model (CHM) to point observations. Mott et al. (2008) evaluate the Alpine3D system (Lehning et al., 2006) comparing simulation with an interpolated map of snow height measurements. The use of interpolation methods in Mott et al. (2008) is justified by the high measurement density of the study area. However, in the majority of other study areas, in situ measurements are way too sparse to characterize the complex spatial variability of alpine snow cover (Pepin et al., 2015; Bales et al., 2006; Vernay et al., 2022; Pomeroy et al., 2009). This situation explains the recent use of snow remote sensing (unmanned aerial vehicle, satellite) as a means of spatial evaluation for large-scale snow cover models. Those methods are still limited by the low availability of remotely sensed variables, mainly snow cover fraction and derived variables or snow height. For example, Vionnet et al. (2021) compare CHM snow simulations (Marsh et al., 2020) with airborne Lidar snow height maps as well as Sentinel 2 snow cover maps. Very recently, (Quéno et al., 2023) used Lidar acquired snow height maps to evaluate the ability of the FSM2oshd framework (Quéno et al., 2023) of representing snow accumulation and erosion areas.

In the above-cited studies using the snow height, SWE, or snow presence related variables, the evaluation experiments are generally carried out using a single set of meteorological inputs. However, it is known that meteorological inputs explain an important part of the variability (Clark et al., 2011; Colle et al., 2013; Mott et al., 2018) and uncertainty Raleigh et al. (2015); Günther et al. (2019) in simulated snow depth and SWE. While the evaluations of model inputs and simulated processes are usually conducted separately, they are often interdependent. Thus, it is difficult to determine if potential errors come from the model or the input variable. For instance, a good simulation of snow height requires both accurate precipitation input and a robust snow evolution model. In order to assess the value of a distributed snow model in the presence of uncertainty in the meteorological forcing, this uncertainty has to be accounted for to raise robust conclusions.

To improve the snow spatial variability of the French snow modeling system, Baron et al. (2023) have developed a novel explicit blowing snow transport model, SnowPappus, coupled with the Crocus physical snow simulation model (Vionnet et al., 2012). This model explicitly represents the vertically integrated saltation and suspension mass fluxes, as a function of wind speed and surface snowpack properties simulated by Crocus. This system is implemented on a regular grid to simulate snowpack evolution at a mountain range scale (approx. 100000 km<sup>2</sup>), for multiple snow seasons. Baron et al. (2023) focused on the evaluation of the model at point scale, demonstrating its ability to accurately simulate blowing-snow fluxes and occurrence at observation stations. However, spatial evaluations of simulations on large distributed domains are currently missing.

The goal of this paper is to present a spatial evaluation of the SnowPappus blowing snow simulation framework (Baron et al., 2023), considering the uncertainty of precipitation estimates through different data sources that exhibit contrasted spatial patterns. The evaluation is based on Pleiades snow depth maps (Deschamps-Berger et al., 2020) and Sentinel-2 snow melt-out dates (Gascoïn et al., 2019) and covers three consecutive snow seasons. We discuss the relative influence of precipitation sources, and blowing snow implementation on the simulated snow cover variability and how their interactions can affect the evaluation of a distributed snow model. By using two contrasted horizontal resolution simulations, we also analyze how the unresolved spatial scales of blowing snow can affect simulation results at a 250 m spatial scale. Finally, we emphasize the main challenges to be solved for more advanced evaluations of spatialized snow simulations.



## 90 2 Data and Methods

### 2.1 Study area

The simulation study site is located east of Grenoble in the French Alps (Fig. 1). It covers 902 km<sup>2</sup> including the Grandes-Rousses and Arves massifs. This area exhibits a complex topography, with elevations ranging from 700 up to 3900 meters a.s.l., a wide range of snow and temperature conditions, and different types of landscape features such as valleys, forests, 95 alpine pastures, lakes, and glaciers. In this area, the local knowledge of precipitation flow patterns tells us that most winter storms come from North-Western flows usually giving increased precipitation on western slopes. The study area includes the Col du Lac Blanc observatory (Guyomarc'h et al., 2019) where Baron et al. (2023) evaluated the blowing snow fluxes and occurrence simulated by SnowPappus. It counts 41 distinct ice patches or glaciers of various sizes as defined in the RGI Consortium (2017), forested areas, and three hydroelectric dams which underline the hydrological importance of the area.

100 As our simulation system is only able to represent snow in open areas, the forests, glaciers, lakes, and rivers in the study zone are masked in our simulations and observation datasets. For the forest mask, the BD FORET® V2 dataset has been used (IGN©, 2021a) with a masking threshold of 25% of forested sub-pixel area. Waterways are masked following data from BD TOPO® (IGN©, 2021b). In the valley, the urban areas around the city of Bourg d'Oisans, Allemont, and Saint Michel de Maurienne are also discarded from the analysis.

### 105 2.2 Grid generation and spatial resolution

The simulations are based on two grid resolutions, 30 m and 250 m. Both simulation grids are built using as reference the French 5 m RGE ALTI® digital elevation model (DEM) from IGN© (2021c). The 5 m high-resolution DEM is resampled using the average method to 30 m and 250 m horizontal resolutions using GDAL/OGR contributors (2023). At 250 m resolution, the 902 km<sup>2</sup> full simulation area is composed of 14 443 grid points. At 30 m horizontal resolution, the test zone is composed 110 of 1 005 699 simulation points.

A geomorphons classification (or landform) is performed on the 250 m resolution DEM, for a more detailed analysis of simulation domain features. Geomorphons introduced by Jasiewicz and Stepinski (2013) are defined as the fundamental structural elements of a landscape. Here, we used the Whitebox Geospatial (2023) classification tool, an open-source software from 115 Lindsay (2014). The algorithm is based on a line-of-sight analysis with similarities to the more classical topographic position index (TPI). This method identifies a set of topographic patterns corresponding to specific terrain attributes and landform types. The advantage of this type of classification is that it allows topographic information to be conveyed mimicking the result of a classification process carried out by a human analyst. Another advantage of the geomorphons classification is that it adapts to the surrounding terrain and can lead to the identification of landform elements regardless of their scale. Jasiewicz and 120 Stepinski (2013) identify the 10 most common landform elements used for geomorphons classification (peak (summit), ridge, shoulder, spur (convex), slope, hollow (concave), footslope, valley, pit (depression) and flat, illustration can be found in Fig. 3 of Jasiewicz and Stepinski (2013)). This allows us to generate a simple, intuitive, and scale-independent landform map of our

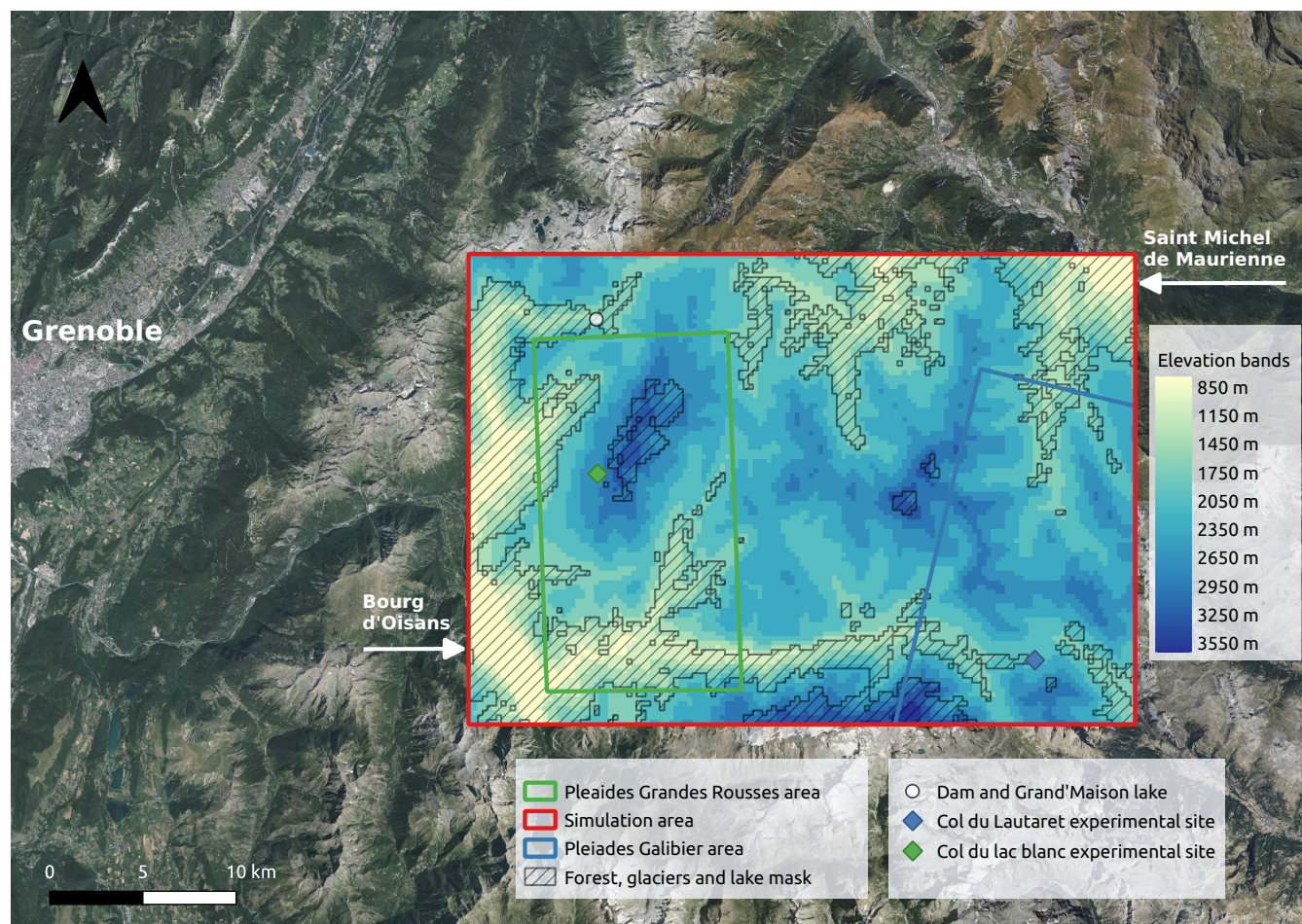


**Figure 1.** Map of the simulation domain (red) and evaluation areas (Pleiades green and blue, Sentinel 2 red). Points of interest are shown as well as forest, glacier, and lake masks. The classification of 250 m pixels is visible with a 300 m step elevation in shades of blue. The summer aerial photography base map is from IGN© (2022).

simulation domain (Jasiewicz and Stepinski, 2013). Figure 2 illustrates the geomorphons classification result (called landform  
classification in the following) of each 250 m grid cell of our simulation domain in terms of the 10 most common landform  
125 elements. Figure 3 illustrates the elevation distribution of the landform elements of our simulation domain. No landform feature  
corresponding to Jasiewicz and Stepinski (2013) 'Shoulder', 'Footslope', and 'Flat' are found in our simulation domains. Fi-  
nally, Appendix Fig. A1 demonstrates the good representativeness of the landform features frequency of our domain compared  
to the entire French Alps and Pyrenees.

For our analysis, each 250 m simulation grid cell is classified in terms of landform types (see Fig. 2) and into 300 m elevation  
130 bands (see Fig. 1).

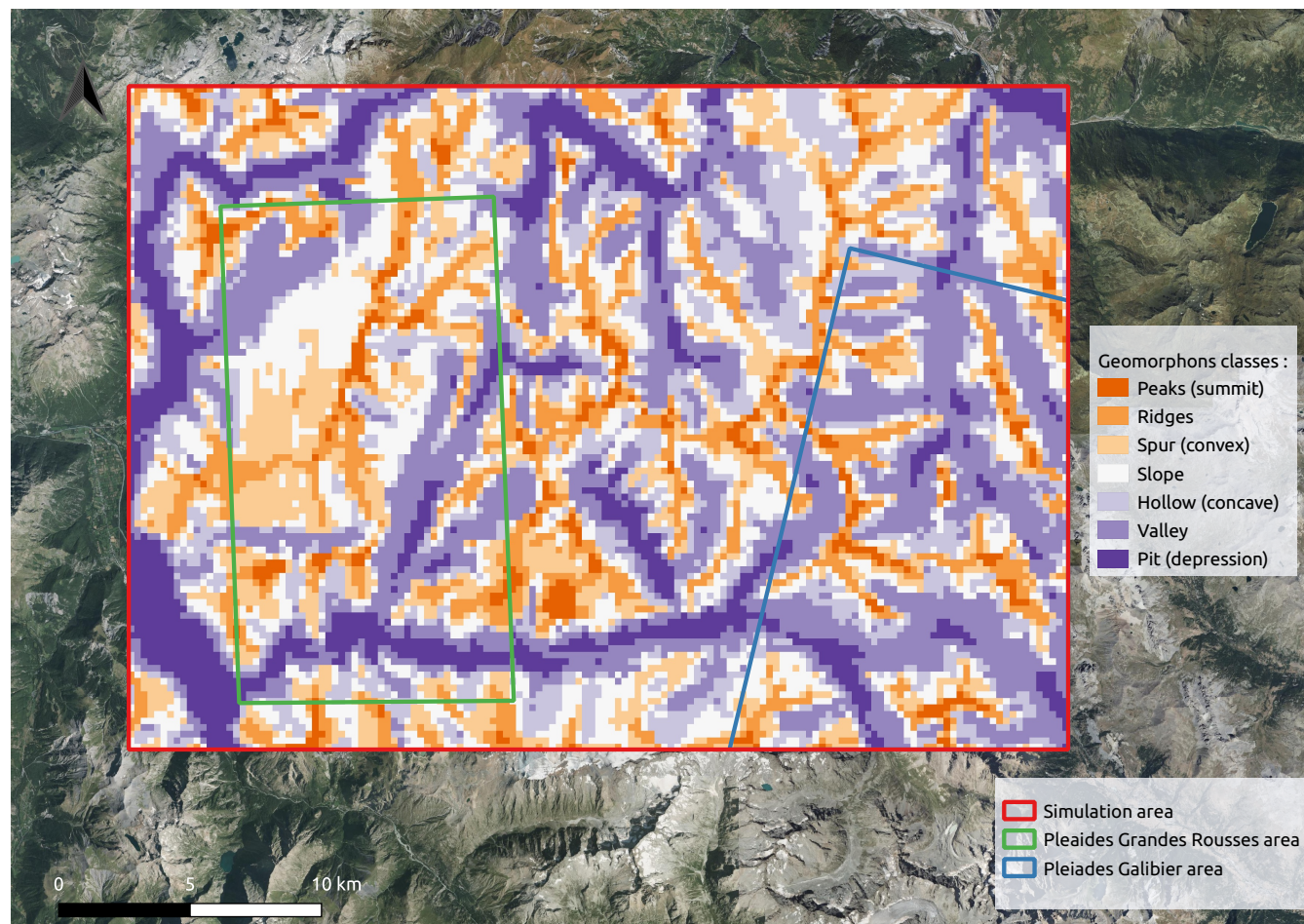


**Figure 2.** Map showing the result of the landform classification performed on our 250 m simulation domain. Each grid cell is classified in terms of the 10 most common landforms described by Jasiewicz and Stepinski (2013). (Peak (summit), ridge, shoulder, spur (convex), slope, hollow (concave), footslope, valley, pit (depression), flat) In our domain, flat, footslope, and shoulder landforms are not present. The summer aerial photography base map is from IGN© (2022).

### 2.3 Crocus snow model

This paper uses the well-established 1D snow model Crocus (Brun et al., 1989; Vionnet et al., 2012), used operationally by the French weather forecast agency (Météo-France), in support of avalanche hazard forecasting (Morin et al., 2020). This snow model relies on a dynamical layering of the snowpack and an explicit representation of snow metamorphism and microstructure up to 50 snow layers (Vionnet et al., 2012). The Crocus snow model is coupled to the ISBA ground and land cover model and is embedded in the SURFEX modeling framework (Decharme et al., 2011; Masson et al., 2013). The snowpack is simulated on a squared grid of 250 m or 30 m spacing. Simulations are run over 3 years, starting from 02 August 2017 06:00

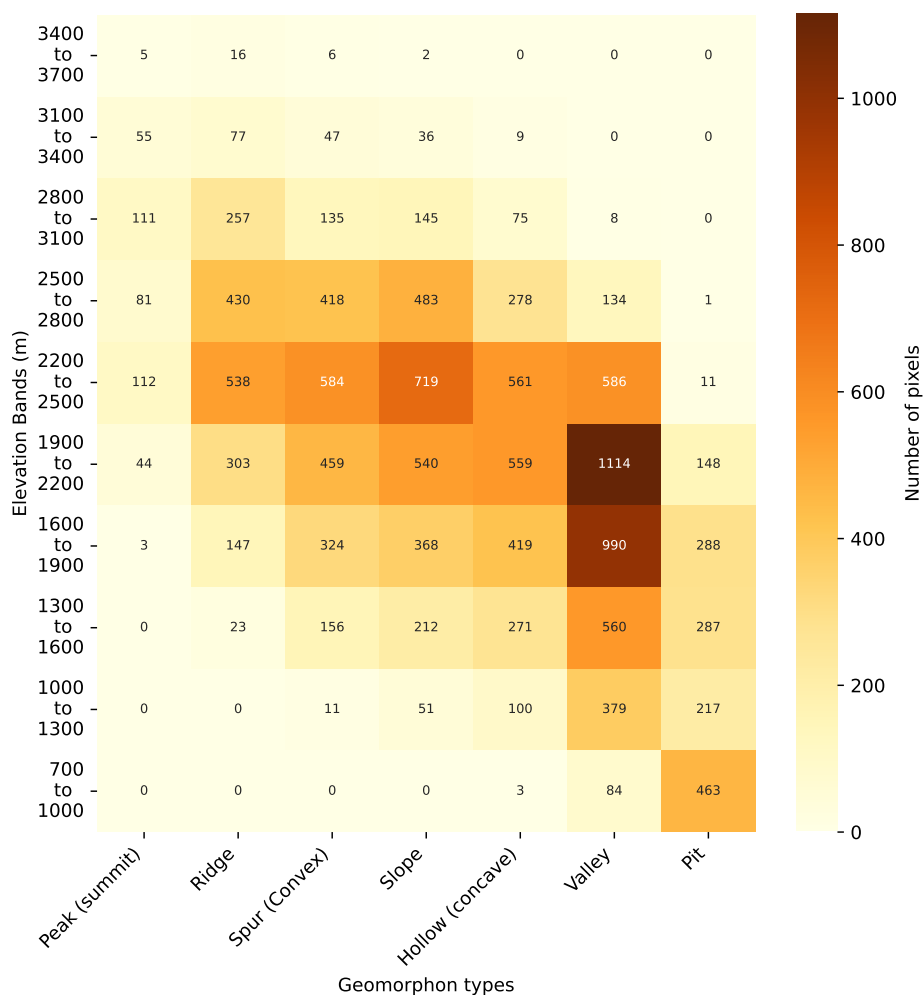


**Figure 3.** Distribution of simulation pixels in terms of 300m step elevation bands and the landform classification. The number of pixels corresponding to each class is shown.

to 02 June 2020 06:00, using a 15-minute time step. The initial ground conditions are taken from a 10-year (2007-2017) simulation driven by the SAFRAN reanalysis (Vernay et al., 2022).

#### 140 2.4 SnowPappus blowing snow model

The SnowPappus blowing snow model has been specially developed to describe snow variability due to blowing snow when the Crocus model is applied in the range of 25 m to 250 m horizontal resolutions (Baron et al., 2023). SnowPappus model simulates blowing snow occurrence, horizontal transport fluxes, and blowing snow sublimation rate on each grid cell as a function of 2D atmospheric forcing and snow surface properties. Then, a blowing snow mass balance is used to quantify eroded or accumulated



145 snow amounts and modify the simulated snow profiles accordingly. Model methods and parameterizations used to represent the different blowing snow processes are described in detail and discussed against existing literature in Baron et al. (2023).

SnowPappus can run over multiple snow seasons and very large domains, in the  $10^5$  km<sup>2</sup> (at 250 m resolution or  $10^6$  simulation points) in a reasonable computing time (half a day on a single computing node, depending on simulation outputs).

## 2.5 Meteorological forcings

### 150 2.5.1 SAFRAN simulations

As most spatialized applications of the Crocus snow model over the French Alps, our simulations are forced by the SAFRAN meteorological reanalysis (Vernay et al., 2022). The SAFRAN analysis system uses as a background, vertical profiles of air temperature, humidity, and the precipitation fields of the ARPEGE NWP system and assimilates near-surface meteorological observations to generate, with an hourly time step, the typical sets of inputs required by a snow model such as Crocus (Durand  
155 et al., 1993). The SAFRAN reanalysis provides these meteorological inputs over 23 climatologically homogeneous areas (named massifs) covering the whole French Alps (Vernay et al., 2022). Here, only the SAFRAN reanalysis corresponding to the Grandes-Rousses massif was used to build the simulation meteorological forcing. For a distributed use, the SAFRAN analysis is linearly interpolated as a function of elevation, for each simulation point (as in Vionnet et al. (2016)) to match the gridded geometry of our simulation domain. Solar radiations are projected according to the slope inclination and aspect  
160 of each pixel and masked in the case of shadows from the surrounding topography similarly to Revuelto et al. (2018) and Deschamps-Berger et al. (2022). In SAFRAN, all meteorological variables are assumed to be constant inside a massif for a given elevation. Whereas large-scale biases are low thanks to the assimilation of numerous gauges observations (Vernay et al., 2022), a large part of the spatial variability of precipitation remains unresolved under this assumption (Vionnet et al., 2016; Quéno et al., 2016; Vionnet et al., 2019; Deschamps-Berger et al., 2022). Therefore, other precipitation estimates are also  
165 considered in this study, respectively from AROME NWP system and ANTILOPE radar-based analysis. An illustration of the mean daily SAFRAN precipitation spatial variability can be seen in Appendix Fig. B1 (a). This map informs us of the spatial and inter-model variability and of the absolute precipitation values of each precipitation dataset.

### 2.5.2 AROME precipitation simulations

AROME is the high-resolution non-hydrostatic NWP system operated by Meteo-France for short-range forecasts. It uses a  
170 1.3 km grid spacing (Seity et al., 2011). Due to high temperature and radiative biases of AROME in mountain areas (Quéno et al., 2020; Gouttevin et al., 2023), and to focus our study on the uncertainty of precipitation spatial patterns rather than on all meteorological forcing uncertainties, we only consider in our simulations only the precipitation amount from AROME. Thus, the precipitation phase is set to solid if the SAFRAN air temperature is lower than 274.15 K and liquid if the air temperature is above 274.15 K. Although more advanced and continuous phase functions are available in the literature (Froidurot et al.,  
175 2014; Vionnet et al., 2022), this choice was made for consistency between all simulations, as this threshold is also used by



the SAFRAN system. SAFRAN analysis data are used for all the other forcing variables. An illustration of the mean daily AROME precipitations can be seen in Appendix Fig. B1 (d).

### 2.5.3 ANTILOPE precipitation simulations

ANTILOPE is an hourly precipitation estimation analysis product (rain rate), combining radar and rain/snow gauges with  
180 0.01° (1 km) resolution (Champeaux et al., 2009). ANTILOPE precipitation fields are the kriging result of available gauge  
measurements, using radar-estimated precipitation fields as external drift. In a mountainous context, the skill of the product  
can be affected by a partial or total mask of the radar beams and other common radar measurement errors (Faure, 2017; Yu  
et al., 2018), although the use of observations improves the precipitation estimates compared to raw radar precipitation. Since  
ANTILOPE doesn't discriminate solid from liquid precipitations, we used information from SAFRAN to classify rainfall and  
185 snowfall as well as all the other forcing variables. The precipitation phase is set to solid if the SAFRAN air temperature is  
lower than 274.15 K and liquid if the air temperature is above 274.15 K. SAFRAN analysis data are used for all the other  
forcing variables. An illustration of the mean daily ANTILOPE precipitations can be seen in Appendix Fig. B1 (c).

### 2.6 DEVINE wind downscaling model

Wind fields are important drivers of turbulent and mass exchanges at the surface of the snowpack. Wind fields also profoundly  
190 determine the onset and evolution of drifting and blowing snow episodes. The interaction between mesoscale winds and local  
topography induces strong modifications both in terms of speed and direction that deeply influence the spatial variability of  
wind fields at the local mountain scale (Whiteman, 2000). Neither interpolated NWP systems operating with a km resolution  
(Seity et al., 2011) nor massif-scale SAFRAN reanalyses (Vernay et al., 2022) would permit us to take into account the local  
influence of terrain on wind fields. As the local scale wind patterns are crucial to determine high-resolution snow patterns  
195 (Musselman et al., 2015), we downscaled AROME wind fields (1.3 km grid spacing) down to a 30 m grid using the DEVINE  
downscaling model (Le Toumelin et al., 2022). This method leverages a convolutional neural network to emulate the behavior  
of the complex atmospheric model ARPS, previously run on a large number of synthetic topographies and in turn increase the  
spatial resolution of wind fields in complex terrain.

The DEVINE downscaling model has been previously evaluated over a large number of in-situ stations (Le Toumelin et al.,  
200 2022, 2023), including stations located in our study domain. It has been shown that DEVINE wind outputs can represent wind  
acceleration along ridges and summits, deceleration windward, and some deflection around topographic obstacles but can not  
represent more complex wind patterns such as thermal winds or recirculation areas.

### 2.7 Model experiments

To disentangle the impacts of the simulation of blowing snow from the precipitation forcing, 250 meter resolution simulations  
205 were run with and without the SnowPappus transport module and with the 3 different precipitation datasets, resulting in 6  
different 250 m simulations. All simulations utilize the default options, the GM98 parametrization of blowing snow occurrence,



and the flux limiter is activated (Guyomarc'h and Mérindol, 1998; Baron et al., 2023). In addition, blowing snow sublimation is activated using SBSM-like equations (Essery et al., 1999; Baron et al., 2023). To investigate the role of unresolved transport variability of snow transport, 2 additional simulations were done at 30 m resolution with and without the SnowPappus transport module (see HR standing for High Resolution). Due to the higher numerical cost of these simulations and the increased complexity of downscaling and validating weather forcing at this resolution, 30 m resolution simulations were only run with the SAFRAN precipitation fields.

As the 30 m resolution simulations are used in this paper to evaluate the contribution of unresolved spatial variability in 250 m simulations, we do not evaluate 30 m simulations at their native resolution but after a resampling on the 250 m resolution grid using ESMF first-order conservative method (Earth System Modeling Framework et al., 2023).

Regardless of the simulation configuration, 10-year SAFRAN spinup simulations (without SnowPappus) were performed to produce the ground's initial condition.

A summary of all the simulation experiments is found in Table 1:

Experiment name	Precipitation forcing	Blowing snow transport mode	Computing resolution
Safran	SAFRAN	No transport	250m
Safran with transport	SAFRAN	Transport	250m
Safran HR	SAFRAN	No transport	30m
Safran HR with transport	SAFRAN	Transport	30m
Arome	AROME	No transport	250m
Arome with transport	AROME	Transport	250m
Antilope	Antilope	No transport	250m
Antilope with transport	Antilope	Transport	250m

**Table 1.** Overview of the different simulation experiments, their model configurations and naming. Important note, the computing resolution is different from the evaluation resolution. All simulations are evaluated at 250m resolution (see Sect. 2.8).

## 2.8 Reference dataset and evaluation methods

### 2.8.1 Sentinel-2 snow melt-out dates

We use the annual snow melt-out dates (SMOD) distributed by Theia (level 3 product of the Snow collection Gascoin et al. (2019)). This product has a 20 m spatial resolution and indicates the last date of the longest continuous snow period. It is obtained by the linear interpolation in the time dimension of all the single-date (level 2) snow cover area products between 1 September and 31 August (Gascoin et al., 2019). The SMOD is given in days starting from September 1st. The Sentinel-2 SMOD obtained for our simulation domain is resampled from the 20 m horizontal resolution to the 250 m resolution grid using the Earth System Modeling Framework et al. (2023) (ESMF) first-order conservative method.



We use the same definition to compute the SMOD from the model output. To compute the longest continuous snow period, the snow height is first averaged by day and then a snow height threshold of 20 cm is applied, as this value was found to be optimal in the sensitivity analysis of Deschamps-Berger et al. (2022) at the same horizontal resolution. The forest, glaciers, and lakes on the domain are masked out both for the Sentinel-2 observations and simulations using the mask defined in Fig. 1 and Sect. 2.1.

### 2.8.2 The Pleiades stereo-imagery

In order to evaluate more directly the spatial variability of the simulated snow height, we used snow height maps derived from Pleiades stereo-images (Deschamps-Berger et al., 2020; Marti et al., 2016). In both cases, snow height is defined following a vertical axis. Pleiades images have a 0.5 m resolution and are acquired on request. Snow height maps are obtained by combining two surface elevations of the same area derived from pairs or triplets of Pleiades images. A reference snow-free surface elevation is acquired during the summer. A winter image acquisition gives a second elevation map with snow on the ground. The difference between the two elevation fields provides a snow height map. Two observation zones have been selected based on available images. The first one covers 66 km<sup>2</sup> around the Col du Lac Blanc experimental site in the Grand-Rousse mountains. The second observation zone covers 168 km<sup>2</sup> around the Lautaret experimental site in the Galibier mountains. Two dates with snow on the ground have been analyzed for each observation zone. For the Grandes Rousses area, two images are available for a different year but at the same period of the season (Pleiades 1 on 13 May 2019 and Pleiades 2 on 4 May 2020). For the Galibier area, the two images give a view at different times of the same season (Pleiades 3 on 23 January 2018 and Pleiades 4 on 16 March 2018).

Because of the method used to reconstruct the snow height map, usual Pleiades observations contain a few no-data pixels where the quality of the observation is lower due to cliffs, steep slopes, clouds, or shaded areas. The snow height map was filtered to exclude values out of the [-0.5 m; 20 m] range. According to previous Pleiades snow maps evaluations (Deschamps-Berger et al., 2020), averaging 2 m Pleiades observation resolution to 250 m reduces the vertical snow height standard error between 0.3 and 0.4 m. Negative snow heights are kept as removing them would slightly positively bias the averages. For comparison with snowpack simulations, the 2 m resolution Pleiades snow depth map is resampled to the 250 m horizontal resolution grid using a conservative method, similarly to (Deschamps-Berger et al., 2020). The entire 250 m pixel is set to No Data if more than 70% of the 2 m pixels is No Data.

The forest, glaciers, and lakes on the domain are masked both for the Pleiades observations and simulations using the mask defined in Sect. 2.1. An additional mask of the No Data pixels in the Pleiades data is applied to the simulations for accurate comparison.

### 2.8.3 Observation data summary

All observations are summarized in Table 2. For the comparison with simulations, the observed SMOD and snow height are grouped by altitude in various elevation bands. The reference altitude used for the observation is the 250 m DEM described in Sect. 2.2. This elevation band classification is one of the most often used in the literature because the elevation is one of the



260 main topographic drivers of snow cover variability (Grünwald et al., 2014; Vionnet et al., 2022; Monteiro et al., 2022; Tong et al., 2009; Deschamps-Berger et al., 2022; Vionnet et al., 2017). However, for a more advanced analysis of the snow cover spatial structure, we also present our results grouped according to the landforms presented in Sect. 2.2.

Satellite observation	Observed area	Variable	Observation date	Native resolution	Aggregated resolution
Pleiades 1	Grandes Rousses region (GR)	Snow height (m)	13 May 2019	2 m	250 m
Pleiades 2	Grandes Rousses region (GR)	Snow height (m)	4 May 2020	2 m	250 m
Pleiades 3	Galibier region (Glb)	Snow height (m)	23 January 2018	2 m	250 m
Pleiades 4	Galibier region (Glb)	Snow height (m)	16 March 2018	2 m	250 m
Sentinel 2 A	Entire simulation domain	SMOD (days)	1 September 2017 to 1 september 2018	20 m	250 m
Sentinel 2 B	Entire simulation domain	SMOD (days)	1 September 2018 to 1 September 2019	20 m	250 m

**Table 2.** Summary of satellite observations used in this study. The observed area, variables, resolutions, and dates are detailed for each observation. The aggregated resolution reminds the resampling operation done on the observation data before comparison with simulations.

## 2.9 Synoptic scores

To summarise the simulation and observation comparison, a combination of three scores has been chosen. The mean bias, standard deviation ratio, and Spatial Probability Score value (SPS) are used to quantify the similarity between the simulated and observed snow height distribution.

The mean bias (MB) defined in Eq. 1 describes the mean bias between the simulation and the observation over a given area.

$$\text{MB}(\text{S}) = \langle \text{S} \rangle - \langle \text{O} \rangle \quad (1)$$

where  $\langle \text{S} \rangle$  represents the mean value of the simulation distribution and  $\langle \text{O} \rangle$  the observation distribution.

270 The standard deviation ratio (or  $\sigma$  ratio in the following) (Eq. 2) is the ratio between the simulated standard deviation and the observed one.

$$\sigma \text{ ratio}(\text{S}) = \frac{\sigma(\text{S})}{\sigma(\text{O})} \quad (2)$$

with  $\sigma(\text{S})$  the simulated standard deviation and  $\sigma(\text{O})$  the observed standard deviation.

The Spatial Probability Score (SPS) is a distance metric between two Cumulative Distribution Functions (CDF) defined in Eq. 3 as the quadratic discrepancy measure between the simulated CDF, noted  $F$  and  $P_{obs}$  the empirical observed CDF. This score is derived from the Continuous Ranked Probability Score (CRPS) primarily used to evaluate probabilistic forecasts in ensemble forecasting (Candille and Talagrand, 2005). Here, it is used to compare two spatial distributions, similarly to the description in Goessling and Jung (2018), although using a non-binary probability field for the perfect observation. In short, this metric quantifies the similarity of two probability densities. It is close to the Wasserstein distance (Rüschendorf, 1985) used in (Vionnet et al., 2021) although here of order 2. A low SPS value means a small distance between the observed and the simulated distributions. Two identical distributions give an SPS score of 0. The SPS unit is identical to the unit of the target variable (m for snow height, days for SMOD).



$$\text{SPS}(F) = \int_{\mathbb{S}} (F(x) - P_{obs}(x))^2 dS. \quad (3)$$

with  $x \in S$ , and  $S$  the volume of possible values of the indicator of interest.

## 285 3 Results

### 3.1 Spatial variability of the snow height

This section compares observed and simulated snow height from the 8 experiments described in Table 1 to the 4 Pleiades observations (Table 2).

#### 3.1.1 Grandes Rousses area

290 First, Fig. 4 illustrates snow height simulations and observations on 13 May 2019. It shows from one side the impact of the SnowPappus blowing snow model on the simulated snow height, where we can see areas of increased and decreased snow height, most visible along the ridges and peaks, and from another side, the major impact of precipitation forcing on the resulting snow height, more specifically for the AROME experiment Fig. 4 b). Additional maps for the 13 May 2019 comparing resolutions can be found in Appendix Fig. C1.

295 For a quantitative evaluation of these snow height maps, we summarized simulations and observations in terms of spatial distributions. For each Pleiades subdomain, simulated snow heights are discretized using 300 m elevation bands. Each snow height distribution describes the internal snow height spatial variability within each elevation band. The associated spatial distributions obtained in the Grandes Rousses region (green box in Fig. 1) are compared in Fig. 5 (a-b) for 13 May 2019 and 4 May 2020. The skill of these distributions is summarized through synthetic scores presented in Fig. 6 (a-b-c-d-e-f).

300 Figure 5 (a) shows a major impact of the precipitation input on the simulated snow height distribution, regardless of the use of snow transport in simulations. Precipitation inputs impact the simulated snow height distribution's shape, variance, and mean value. Simulation with AROME precipitations leads to the highest snow height on average, for all elevation bands and the two evaluation dates. This result is especially notable for Fig. 5 (a) at the elevation band of 2500 to 2800 m on the 13 May 2019 evaluation. The AROME precipitation gives a mean snow height of about 3 m representing a positive bias compared  
305 to the Pleiades observations mean (1.87 m), consistently with Fig. 6 (a). The standard deviation of the AROME simulations overestimates Pleiades' standard deviation at low elevations on both dates Fig. 6 (b-e). It is more realistic between 2500 and 2800 m, and dependent on snow transport at higher elevations.

Simulations with the ANTILOPE precipitation, on the other hand, have a negative snow height bias compared to the ob-  
310 servation. For the 2500 to 2800 m elevation band, the ANTILOPE simulations give a mean snow height of only 1.30 m. This negative bias tends to increase with altitude as illustrated in Fig. 6 (a). The standard deviation of ANTILOPE simulations is

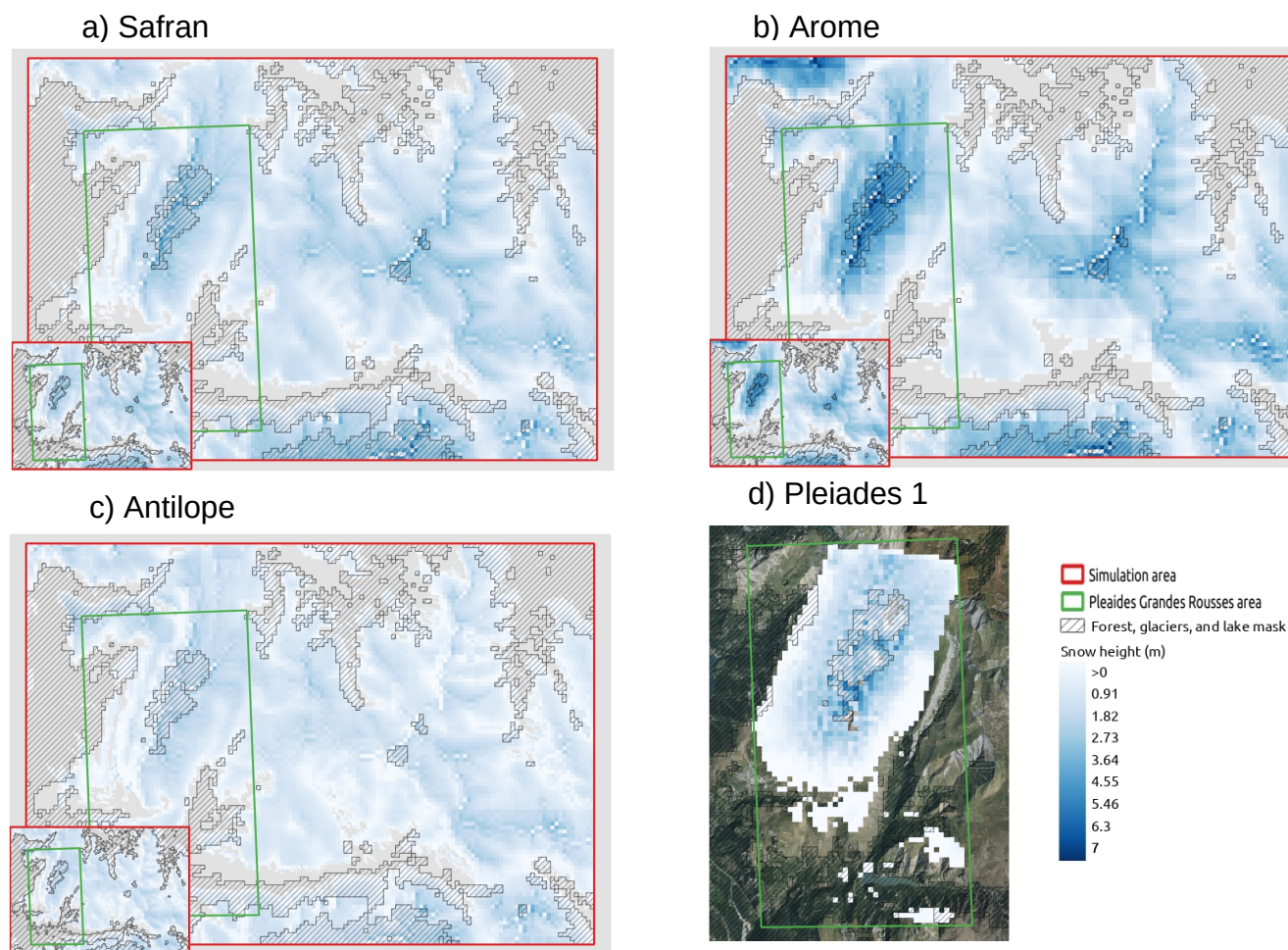


**Figure 4.** Map of simulated and observed snow height on the 13 May 2019 10:00. (a) Safran 250 m simulation with snow transport and without snow transport in the left submap. (b) Arome 250 m simulation with snow transport and without snow transport in the left submap. (c) Antilope 250 m simulation with snow transport and without snow transport in the left submap. (d) The Pleiades 1 observed snow height resampled to 250 m. The absence of snow in simulations is indicated in grey. For d) the summer aerial photography base map is from IGN© (2022).

315 closer to observations than AROME simulations. Similar results are found for 4 of May 2020 (Fig. 5 (b), Fig. 6 (d-e-f)). For the SAFRAN and SAFRAN HR simulations, results are consistent between the simulation resolution (250m and 30m) but with varying skill between both evaluation years. The mean simulated snow height for the 2500 to 2800m elevation band (1.90 m) is consistent with observations on 13 May 2019. At all elevations, the SAFRAN and SAFRAN HR simulations show a lower bias compared to observations than simulations forced by AROME and ANTILOPE. However, the SAFRAN mean value of 4 May 2020 (around 2 m) underestimates the observed snow height. A similar result is found at both resolutions and with or

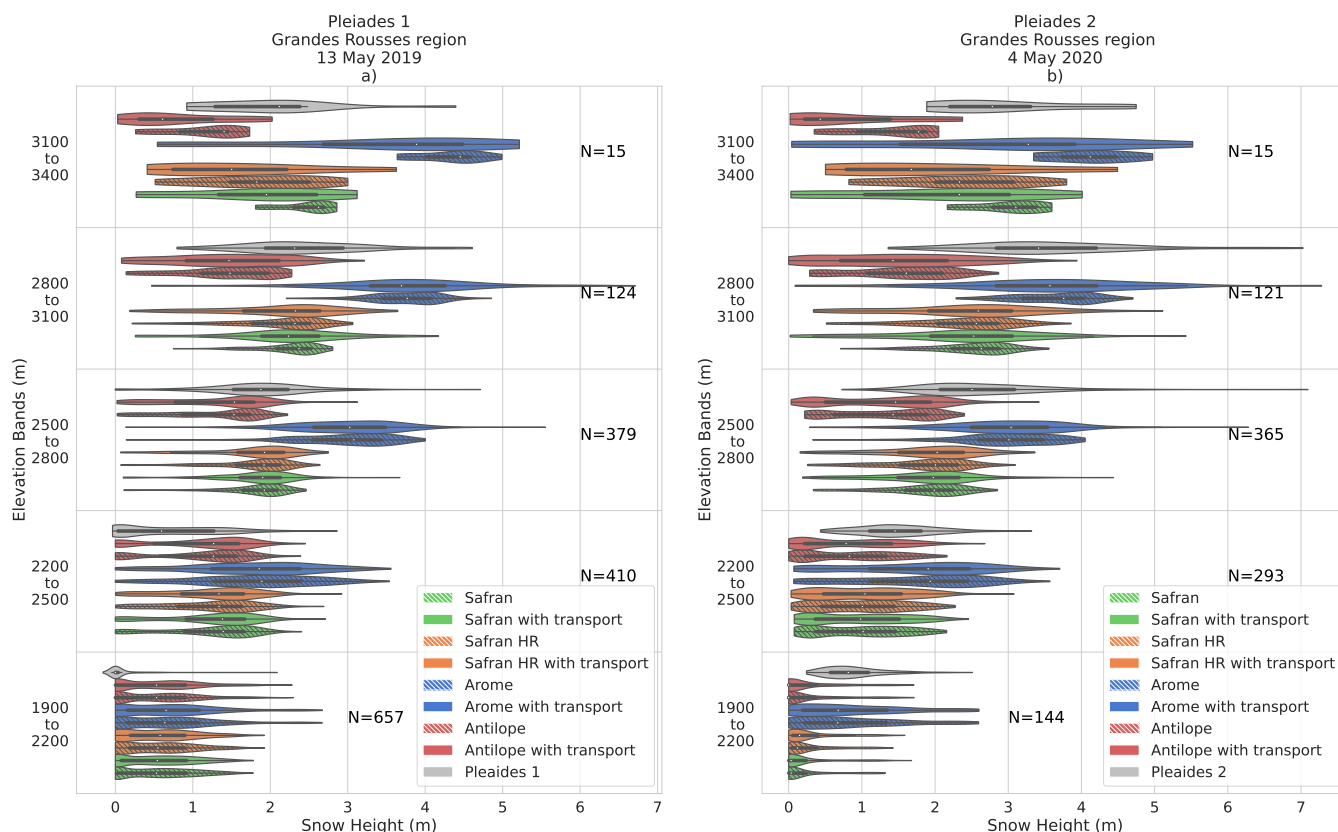


**Figure 5.** Spatial distribution of snow height (m) for 300 m elevation bands in Pleiades observations (gray) and all simulation configurations over the Grandes Rousses mountains on 13 May 2019 (Pleiades 1)(a) and 4 May 2020 (Pleiades 2)(b). The different colors represent the different precipitation forcing and horizontal resolutions while hatching is used to distinguish between the activation and deactivation of the SnowPappus blowing snow scheme.

without snow transport. At most elevations, the standard deviation is similar to ANTILOPE forcing and close to the Pleiades observations.

320

The representation of snow transport is found to only impact snow height bias for the upper elevation band (with a reduction of the mean snow height). The fact that this impact is beneficial or detrimental depends on the choice of the meteorological forcing. Below this elevation band, the impact of snow transport on the bias is found shallow to nonexistent. Figure 5 (a) also shows that for the 3 upper elevation bands (above 2500m), SnowPappus (non-hatched violin plots) increases the simulated standard deviation on average by 63.7% between snow height distribution with and without snow transport (hatched violin plots). Figure 5 (b) (above 2500m) shows a similar standard deviation increase of 67.7% for the next year when adding snow transport in the simulations. The impact of snow transport on the simulated snow height is noticeable for all precipitation inputs. Figure 6 (b-e) shows that the increase of standard deviation (above 2500m) introduced by the transport module is sometimes

325

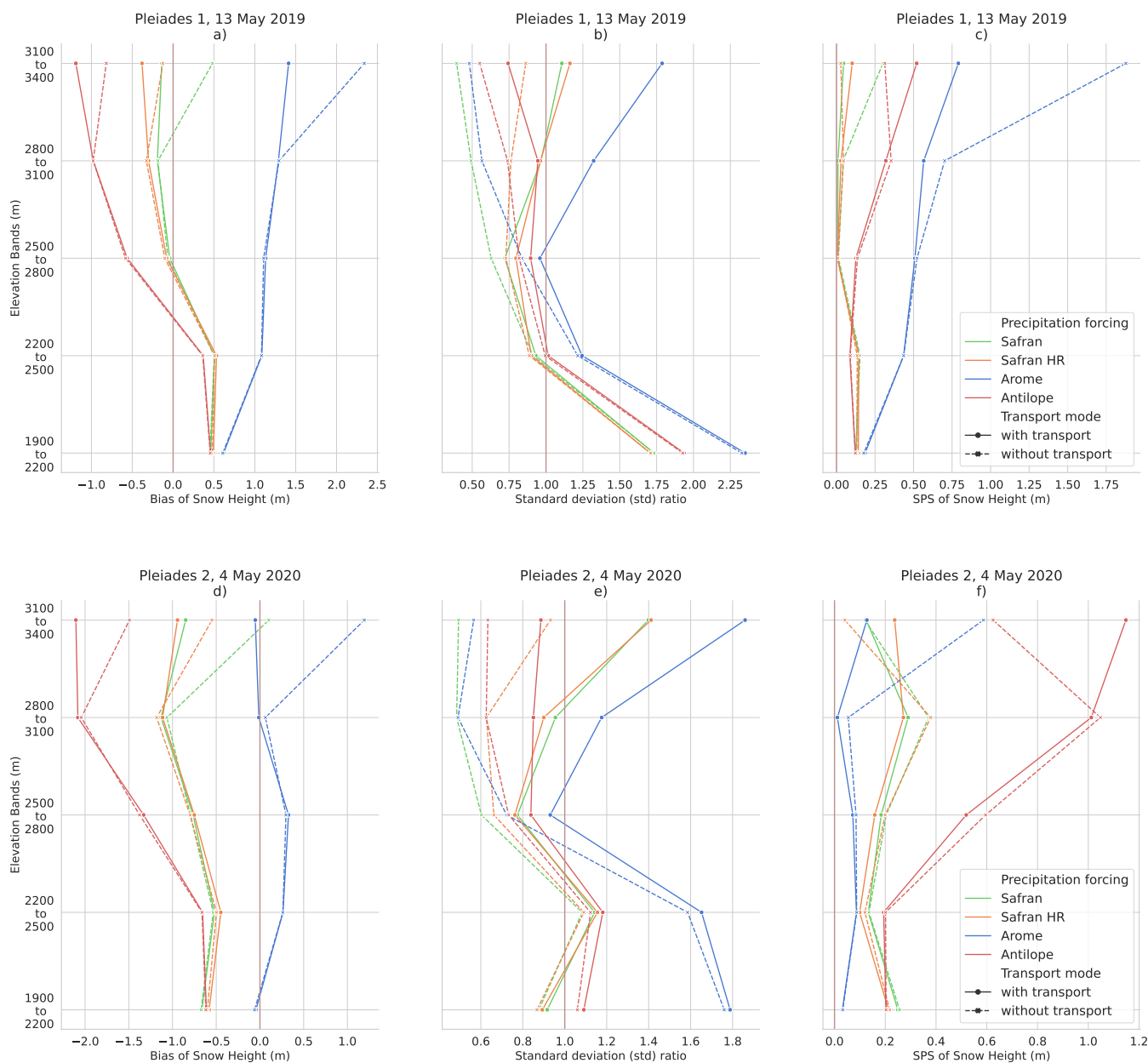


**Figure 6.** Scores comparing simulations with the Grandes Rousses Pleiades observations. (a-b-c) compares simulations with the 13 May 2019 Pleiades 1 image ; (d-e-f) is based on the 4 May 2020 Pleiades 2 image. (a-d) Bias (m) ; (b-e) Standard deviation ratio (no unit) ; (c-f) SPS (m). All scores are presented as a function of 300 m elevation intervals.

overestimated comparatively to the observation ( $\sigma$  ratio  $>1$ ), depending on the date and precipitation forcing. Below 2500 m,



330 the snow height distributions with and without snow transport, for a given precipitation input, are broadly similar.

Finally, SPS scores (Fig. 6 (c-f)) suggest that model performances are mostly modified by SnowPappus at the highest pixels of our domain and that simulation improvements or degradation depend on combinations of model setups (transport/no transport and precipitation forcings). Thus, no optimal precipitation forcing can be identified systematically.

### 335 3.1.2 Galibier area

The second snow height evaluation (Fig. 7 and Fig. 8), is done in the Galibier Mountains area (blue box in Fig. 1). It uses two snow height maps derived from Pleiades stereo-images acquired in January and March 2018, in which snow cover extends to lower elevations than in the Grandes Rousses snow height maps. At both dates, a positive bias appears for the three lowest elevation bands, regardless of the forcing and decreasing with elevation (Fig. 8 (a-d)). For instance, the Pleiades observation  
340 provides a mean snow height of 1.25 m at the 1900-2200 m elevation band on 23 January 2018, while the simulation's mean values are all above 1.74 m of snow. At these elevations, the distribution standard deviation (0.71 m in the Pleiades observations) is underestimated by all simulations (from 0.16 m for SAFRAN to 0.32 m for AROME), without any significant impact of the snow transport module (Fig. 8 (b-e)).

For the two upper elevation bands, the main features are consistent with the evaluations on the Grandes Rousses area: at both  
345 dates, the AROME simulations exhibit the highest mean snow height corresponding to a positive bias compared to observations, while the ANTILOPE simulations exhibit the lowest snow height corresponding to a negative bias. Contrary to the previous section, SAFRAN simulations also overestimate snow height in the Galibier area. For all precipitation forcing, the standard deviation of simulations without transport (between 0.11 m and 0.25 m in January at the upper level) is much smaller than in the observed spatial distribution (0.87 m). When the snow transport is activated, a more realistic spatial variability is obtained,  
350 although it is still underestimated below 2800 m elevation. This conclusion remains valid on 16 March (Fig. 7 (b)). As for the Grandes Rousses evaluation, the simulations with the AROME precipitation have the highest spatial variability in snow height at all elevations and for the two dates. Conversely, the simulations with SAFRAN have the smallest standard deviation across elevation.

For the SPS score (Fig. 8 (c-f)), the ANTILOPE forcing leads to the simulated snow height the closest to the observations  
355 for both dates above 2200 m, contrary to the results over the Grandes Rousses area. For the lowest elevation band, AROME simulation with snow transport is the closest to observations with an SPS score of 0.4 and 0.3 m in January and March. The simulations forced by SAFRAN precipitation provide the spatial distributions the furthest to Pleiades observations. This is an opposite conclusion to the results obtained on the Grandes Rousses region. Therefore, the evaluations on this second region confirm the difficulty of identifying optimal precipitation forcing for all regions, elevations, and dates.

### 360 3.1.3 Summary: Relative impacts of snow transport and precipitation forcing

When comparing the simulation performance between both simulation regions and all dates, common and different patterns arise. The impact of the simulation of snow transport on the bias is restricted to the upper altitude, close to mountain summits.

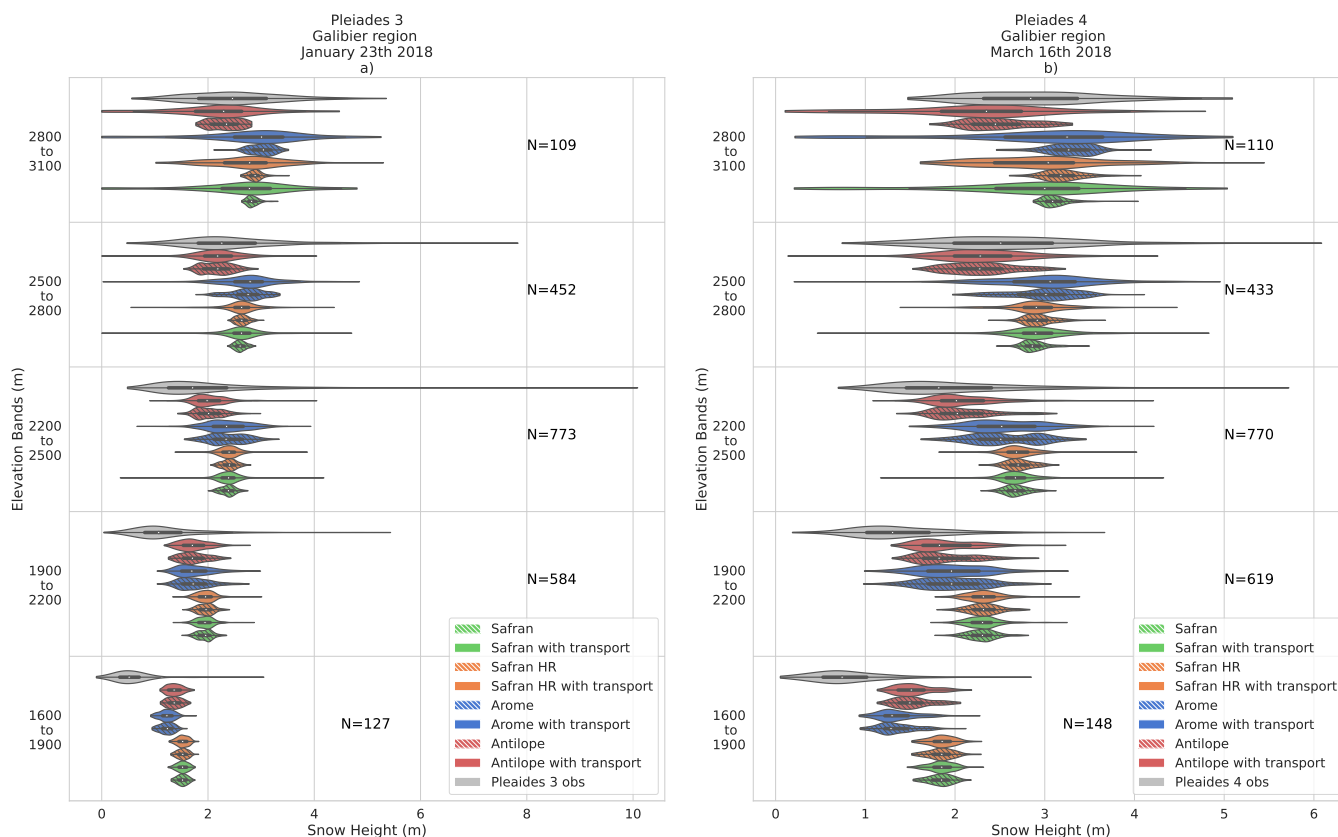


**Figure 7.** Spatial distribution of Snow height (m) for 300 m elevation bands in Pleiades observations (gray) and all simulation configurations over the Galibier on 23 January 2018 (Pleiades 3)(a) and 16 March 2018 (Pleiades 4)(b). Similar legend as in Fig. 5

For all simulations, higher average snow height are obtained without transport than with transport. However, the added value of snow transport can not be established on this criteria as the bias highly depends on the precipitation forcing.

365 In all simulations, lower snow heights are obtained with ANTILOPE precipitation and higher snow heights with AROME precipitation, with increasing differences with elevation. However, no precipitation forcing leads to the simulation of the most unbiased snow heights for all areas and evaluation dates. Across all elevation ranges, the mean driver of simulation bias appears to be the precipitation dataset choice.

370 The addition of snow transport increases and improves the simulated standard deviation, mainly above 2500 m and increases with elevation. For these upper elevation bands, the snow transport prevails in the choice of the precipitation dataset on this criteria. For the lower elevation bands, the main driver of simulation standard deviation appears to be the choice of the precipitation dataset. The simulations using AROME precipitation have the biggest standard deviation value of all simulations.

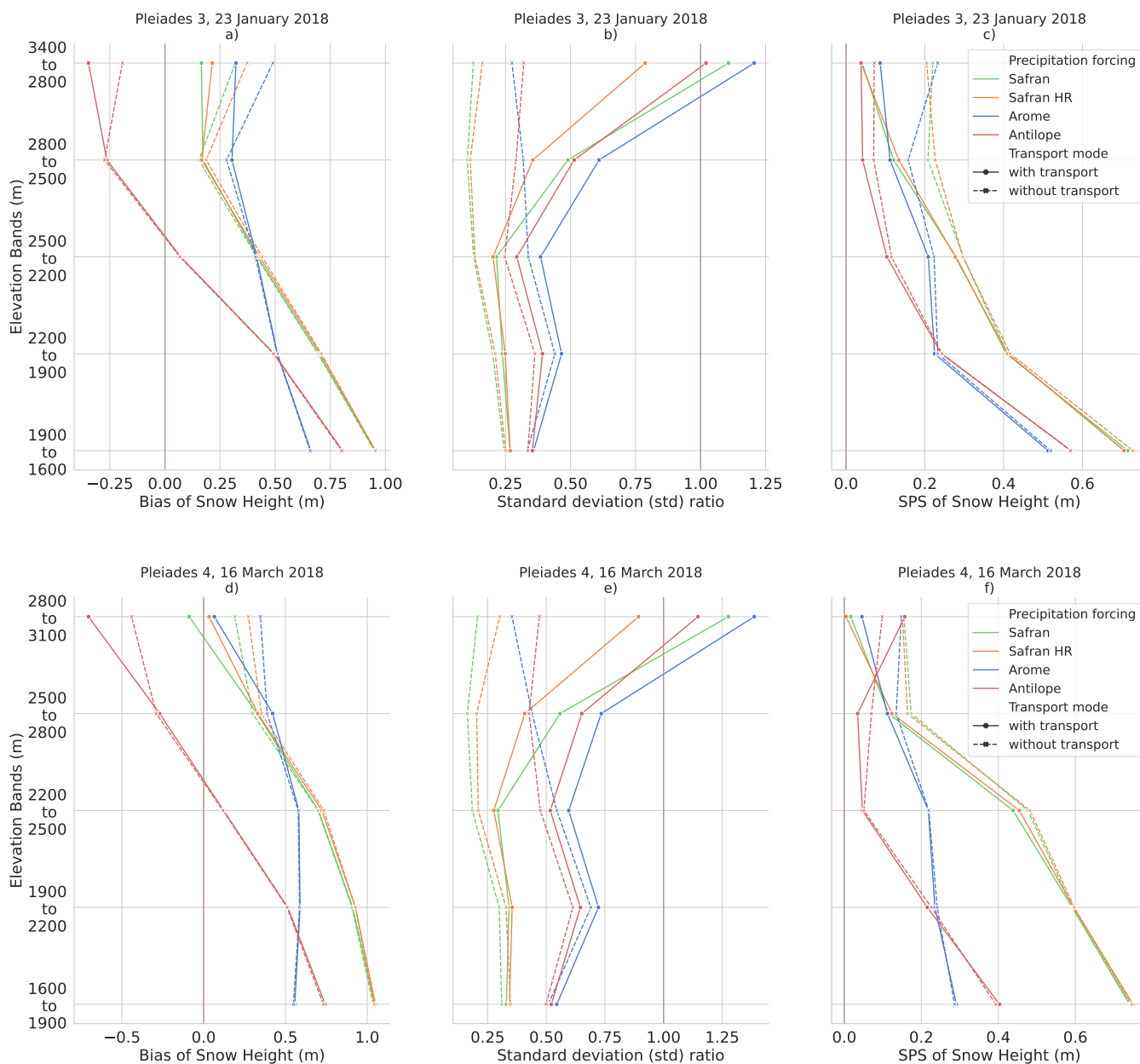


**Figure 8.** Scores comparing simulations with the Galibier Pleiades observations. (a-b-c) compares simulations with the 23 January 2018 Pleiades 3 image ; (d-e-f) is based on the 16 March 2018 Pleiades 4 image. (a-d) Bias (m) ; (b-e) Standard deviation ratio (no unit) ; (c-f) SPS (m). All scores are presented as a function of 300 m elevation intervals.



### 3.1.4 Impact of subgrid variability

The effect of unresolved subgrid variability can be analyzed by comparing SAFRAN and SAFRAN HR simulations. Simulation maps illustrating the expected subgrid variability can be found in Appendix Fig. C1 (a-b-c). At the 30 m grid resolution, the spatial variability of the topography (SAFRAN HR without transport vs. SAFRAN without transport) reduces the snow height and increases the 250 m scale spatial variance at high elevations for the Grandes Rousses evaluations. The impact is smaller for the Galibier assessment.

Resolving snow transport at a 30 m grid resolution (later averaged to 250 m) reduces the impact of snow transport on simulations compared to 250 m simulations (orange dashed and continuous lines are less distant than green dashed and continuous lines). As snow transport tends to decrease snow height and increase spatial variance, the impact of resolving the 30 m scale snow transport has an opposite effect on the resolution of the 30 m scale topography. Finally, SAFRAN HR and SAFRAN simulations are relatively close in terms of snow height bias,  $\sigma$  ratio, and SPS. Therefore, despite the significant impact of the simulation resolution at the process level, it is not obvious that the 250 m simulations would provide less accurate snow height spatial distributions than simulations computed at higher resolution and resampled on a 250 m grid.

## 3.2 Spatial variability of Snow Melt-Out Date (SMOD)

The evaluations of the SMOD allow us to extend the evaluations over our entire simulation domain. It also provides complementary information on the entire snow season than the use of snow height snapshots. The associated spatial SMOD distributions for the 2017-2018 and 2018-2019 years can be found Fig. 9 (a-b). The synthetic summary of simulation performances is given by Fig. 10 (a-b-c-d-e-f).

### 3.2.1 Differences between years

There is a notable difference in distribution variance when comparing the evaluation results for the two years (Fig. 9). In Fig. 9 (b), 2018-2019 modeled SMOD clearly shows a wider variability at every altitude band and for each simulation configuration compared to 2017-2018 (Fig. 9 (a)). Below 2200m, the SMOD spatial variability is also higher in 2018-2019 than in 2017-2018 in Pleiades observations but with less pronounced differences than in simulations.

### 3.2.2 Impact of precipitation forcing

Above 2500 m, the simulation with transport and the ANTILOPE precipitation has the largest distribution variance and lower mean SMOD value. As a result, this is the only simulation that underestimates the SMOD in 2018-2019 (Fig. 10 (d)) and overestimates its spatial variability (Fig. 10 (e)).

For the other precipitation forcing, in 2017-2018 the SMOD is overestimated at low elevations indicating that the snow melt-out occurred too late in the season compared to observation. Conversely, SMOD is underestimated at high elevations with a simulated melting up to 20 days before the observed one. In 2018-2019, SMOD was overestimated at all elevations. On average, the spatial variance of SMOD is underestimated except for simulations with AROME forcing at the two lowest

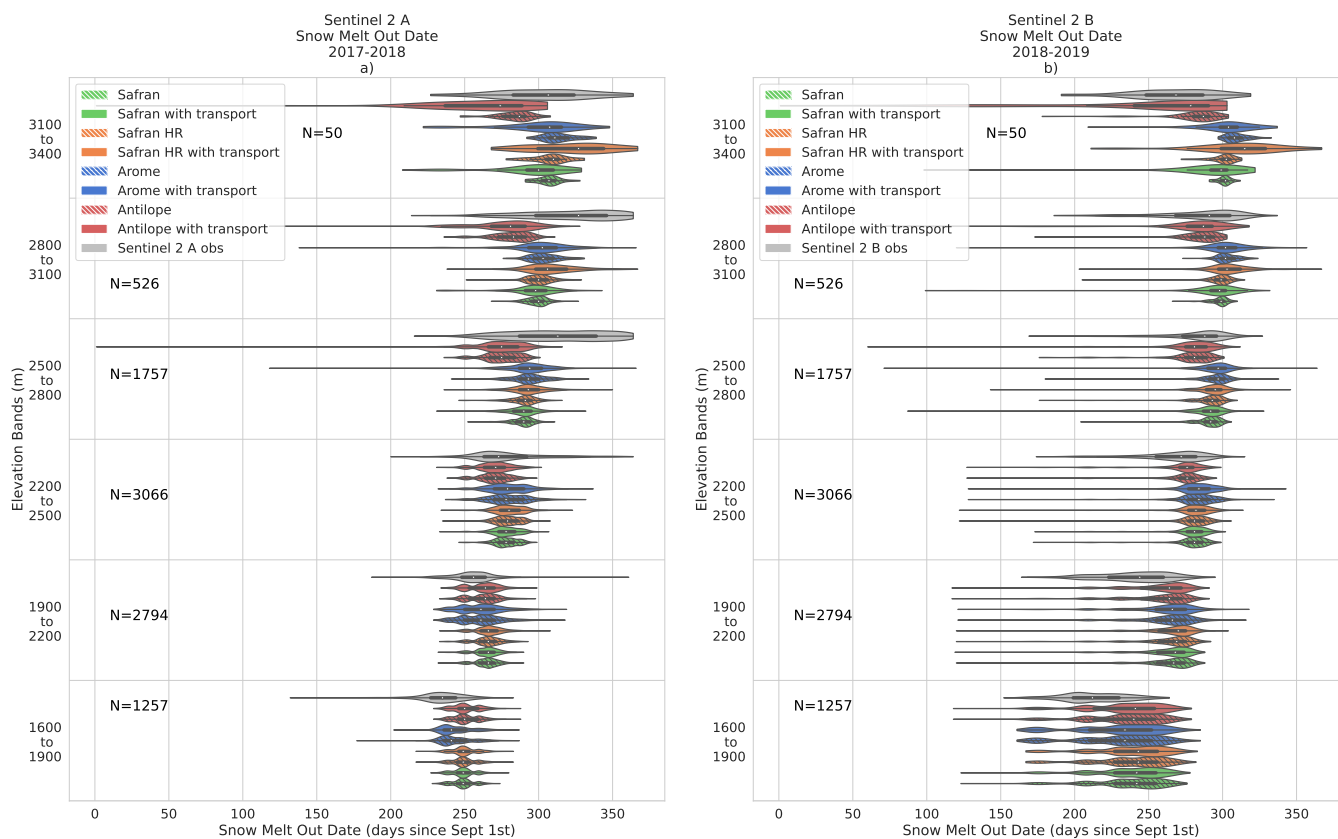


**Figure 9.** Snowpack Melt-Out Date (SMOD) depending on elevation and simulation configuration. The simulations are compared with Sentinel-2 SMOD observations of the full simulation domain, for the 2017-2018 (Sentinel 2 A) and 2018-2019 years (Sentinel 2 B).

elevation bands where the  $\sigma$  ratio is found close to 1. It is interesting to note that in the lowest elevation band Fig. 9 (b), an  
 405 AROME pixel never has a snow height greater than the SMOD threshold during the year (see Sect. 2.8.1) and is therefore given  
 a 0-day SMOD value, contrary to what happens for all the other simulations and the observation.

The SPS values of SMOD (Fig. 10 (c-f)) finally provided the opposite conclusion between both years with the simulations  
 forced by AROME being the closest to the observed spatial distribution at all elevations in 2017-2018 but the furthest in  
 2018-2019 and conversely the simulations forced by ANTILOPE the furthest to observations in 2017-2018 and the closest in  
 410 2018-2019. This result confirms, using SMOD, the conclusion of Sect. 3.1 that no precipitation forcing can be systematically  
 identified as optimal for all evaluation periods and criteria.

### 3.2.3 Impact of snow transport

Figure 9 and Fig. 10 (b) and (e) show an increase in SMOD standard deviation when activating snow transport in simulations,  
 consistent with the increase of snow height variance shown in Sect. 3.1. The standard deviation of simulated SMOD with



415 transport is found to increase with altitude. This increasing spatial variance of SMOD with altitude is also observed with Sentinel 2 imagery, whereas simulation without transport keeps a standard deviation rather similar. Nevertheless, the impact of precipitation forcing on SMOD spatial variability is at least as high as the impact of snow transport. Therefore, the added value of snow transport is still difficult to establish on that criteria, although simulations based on SAFRAN and AROME forcing would suggest that the SMOD spatial variability is improved by the snow transport module.

420 The addition of snow transport also decreases the SMOD for all 250 m resolution simulations, with an increasing impact on altitude. Therefore, concerning the SMOD bias, the impact of snow transport can be either beneficial in 2018-2019 or detrimental in 2017-2018 depending on the sign of the general bias of the simulation without transport.

Except with ANTILOPE in 2017-2018, simulating snow transport always results in improved SPS of SMOD. The detrimental impact of snow transport at high elevations in 2017-2018 for ANTILOPE forcing is probably linked with the much smaller estimates of precipitation by ANTILOPE (Appendix Fig. B1), for which the reasons are discussed in Sect. 4.2.

425

### 3.2.4 Impact of subgrid variability

The addition of snow transport in the 30 m resolution SAFRAN HR simulations increases the SMOD for the two evaluation years while on the contrary snow transport decreases the SMOD in the 250 m resolution SAFRAN simulation. In terms of spatial variance, the increase of spatial variance by snow transport is higher at 250 m resolution than at 30 m resolution. The direct impact of resolving a finer topography in simulations without transport (differences between orange and green dashed lines) is less significant than on snow height evaluations.

430

### 3.3 Impact of landform types

In this section, the spatial simulated distributions of snow heights and SMOD are compared with satellite observations while grouped by landform types instead of elevation bands, as described in Sect. 2.2 and Fig. 2.

435 Figure 11 compares the January and March 2018 Galibier Pleiades images to snow height simulations grouped by landform types. Appendix Fig. D1 presents the same comparison using 13 May 2019 and 4 May 2020 Grandes Rousses Pleiades images. The comparison of simulation with and without transport shows that most of the snow height bias difference (Fig. 11 (a) and (d)) is found on pixels classified as 'Peak (summit)' or 'Ridges'. However, this impact on bias can be either beneficial or detrimental depending on the bias of the simulation without transport, highly dependent on the precipitation forcing, similar to the results described in the analyses based on elevation bands.

440

Simulations with snow transport show lower mean snow height in pixels classified as 'Peak (summit)' and 'Ridges' compared to simulations without transport. Conversely, simulations without snow transport exhibit lower snow height on 'Spur (Convex)', 'Slopes', and 'Hollow (Concave)'. This behavior can be found in each 250 m simulation, regardless of the simulation forcing (Fig. 11, Fig. D1) except for the SAFRAN HR simulations.

445 It can be noticed that the ordering between the different precipitation inputs does not depend on the landforms classes while it was quite dependent on elevation bands.

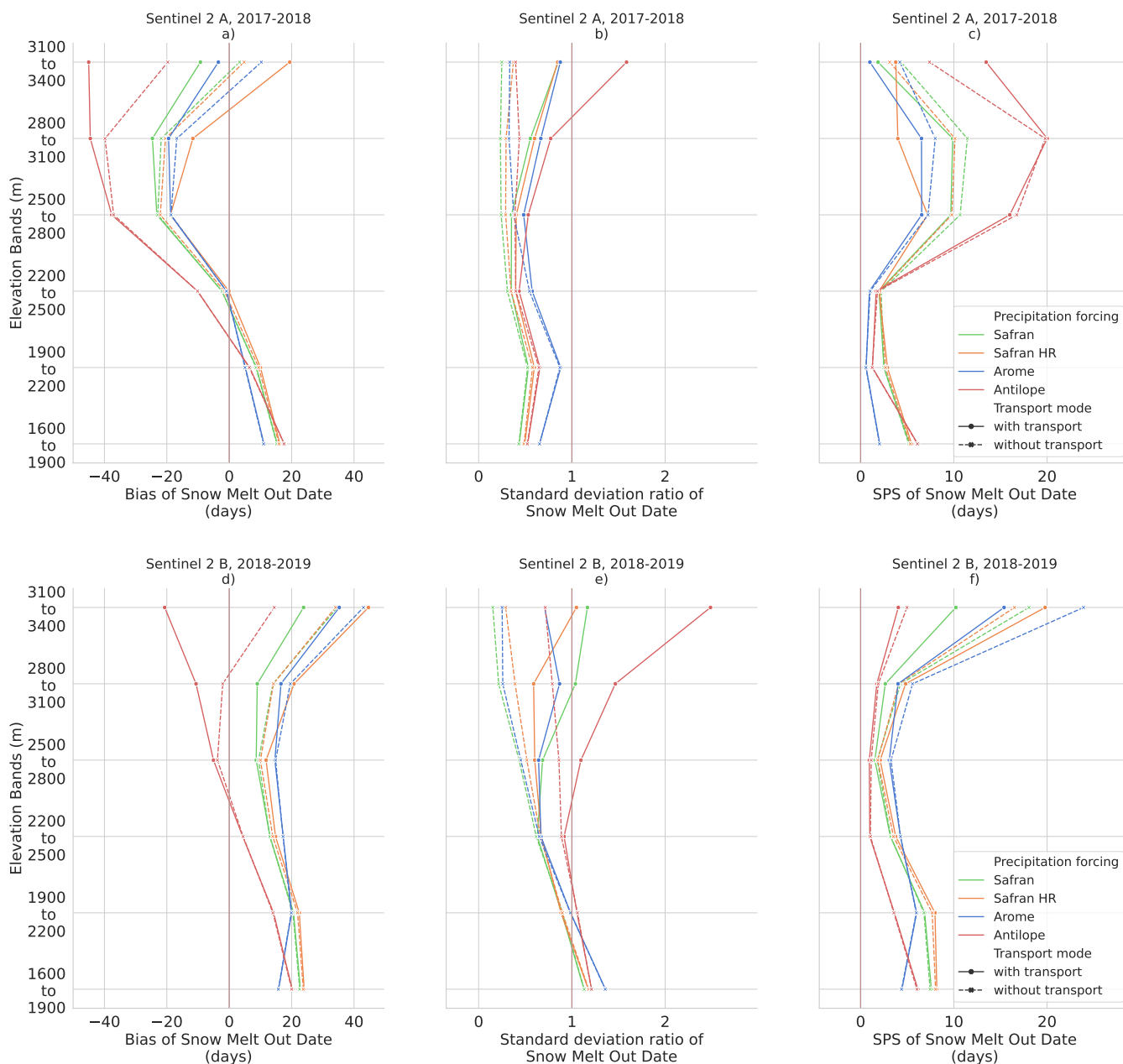


**Figure 10.** Scores comparing simulated SMOD with Sentinel 2 imagery. (a-b-c) 2017-2018 year (Sentinel 2 A) ; (d-e-f) 2018-2019 year (Sentinel 2 B). (a-d) Bias (days) ; (b-e) Standard deviation ratio (no unit) ; (c-f) SPS (days). All scores are presented as a function of 300 m elevation intervals.

For all precipitation datasets, the standard deviation of simulations without transport is much smaller than in the observed spatial distribution. The landforms where the activation of transport has the most impact on snow height variance are (by order

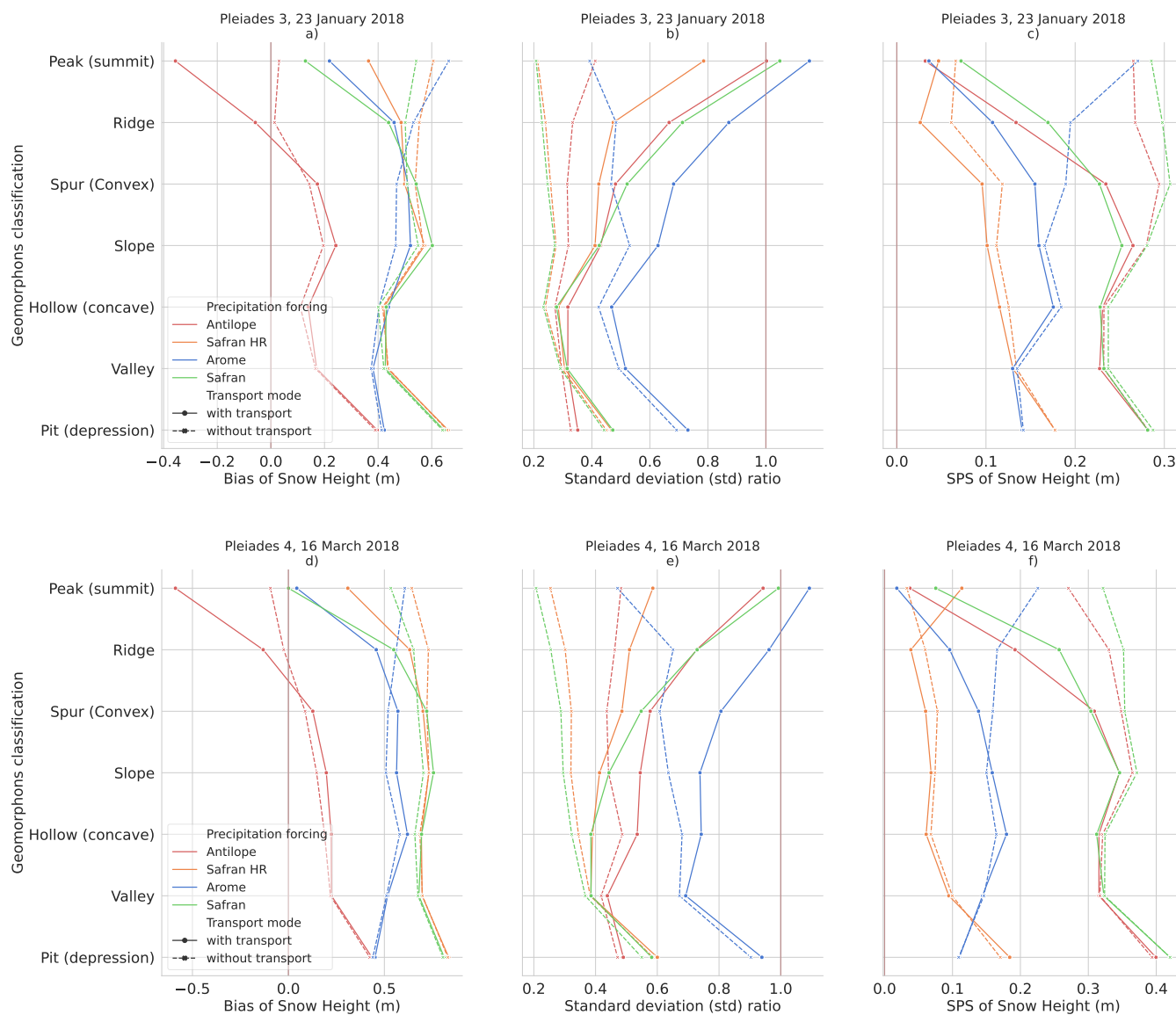


**Figure 11.** Scores comparing simulations with the Galibier Pleiades observations. (a-b-c) compares simulations with the 23 January 2018 Pleiades 3 image ; (d-e-f) is based on the 16 March 2018 Pleiades 4 image. (a-d) Bias (m) ; (b-e) Standard deviation ratio (no unit) ; (c-f) SPS. All scores are presented as a function of landform pixel classifications.

of importance): 'Peak (summit)', 'Ridges', 'Spur (Convex)', 'Slopes' and 'Hollow (Concave)'. Compared to the observed  
 450 variance, this behavior is more realistic when snow transport is activated, Fig. 11 (b) and (e) for all precipitation forcings.  
 While the simulated distribution variance better matches the order of magnitude of the observed one for 'Peak (summit)',  
 'Ridges', and 'Spur (Convex)', the simulated distribution variance of 'Slopes' and 'Hollow (Concave)' is seen to be still half of



the observed one. As for the evaluation using elevation bands, the simulations with the AROME precipitation have the highest spatial variability for the two dates and each landform type. Conversely, the simulations with SAFRAN and no snow transport  
455 have the smallest standard deviation across landforms.

The improvement of the SPS score Fig. 11 (c) and (f) due to the representation of snow transport is major on 'Peaks (summits)' and 'Ridges' and noticeable on 'Spur (convex)' and 'Slope' classes. This improvement is obtained for all precipitation forcings (even in the ANTILOPE case where the bias has deteriorated), therefore mainly driven by the improvement in snow height variance. The SAFRAN HR simulations with and without transport have the lowest (better) SPS values for the two  
460 evaluation dates and most of the landform types while it is not the least biased. A closer look at the simulation's cumulative distribution function (not shown here) shows that the shape of the cumulative distribution is indeed more similar to the observed one (albeit biased). This conclusion differs from the results obtained using a grid cell classification by elevation bands.

Figure 12 presents the two-year evaluation using Sentinel 2 SMOD and landforms. Figure 12 (a-d) show the impact of SnowPappus blowing snow simulations on simulated SMOD. As for snow height in Fig. 11, the impact on SMOD is mainly  
465 limited in areas classified as 'Peak (summit)' or 'Ridge'. SMOD difference when using SnowPappus is found to go up to 20 days for 'Peak (summit)'. When comparing the two evaluation years, similar behavior is found, except the 2018-2019 year appears uniformly more biased. Areas classified as 'Valley' and 'Pit' appear more biased for every precipitation forcing.

In Fig. 12 (b-e), the impact of snow transport is again mainly present on 'Peak (summit)' and 'Ridges' landforms, but with a high variability between both years and a lower impact when AROME precipitation forcing is used (with already a higher  
470 spatial variability even without transport). In 2017-2018, the impact of snow transport is always beneficial on the SMOD  $\sigma$  ratio, as obtained for snow heights, but for the second season, it depends on the precipitation forcing. The simulated standard deviation of AROME simulations appears close to the observed one for all landforms but pixels classified as 'Pit'. This better behavior of AROME was not illustrated in the evaluation done using the elevation bands. The other precipitation forcing appears underdispersed with a standard deviation ratio around 0.5-0.75.

Looking at the SPS scores Fig. 12 (c-f), the impact of snow transport is less clear than for snow heights, similar to the results obtained by elevation bands. SPS values are smaller using landform classification than elevation bands. All simulations appear to have difficulties in representing SMOD distribution in pixels classified as 'Valley' and 'Pit' conversely to results of Fig. 11. The SPS scores are also more similar between the two evaluation years, contrary to the SPS score using elevation bands grouping. Figure 10 (c) shows a distance increase between all simulations and observations distribution between 2500-3100 m.  
480 This effect is not found in Fig. 12 (c). On the contrary to Fig. 11, the SAFRAN HR does not have the lowest SPS values, and AROME simulations'  $\sigma$  ratios are found to be more realistic.

## 4 Discussion

### 4.1 Sources of snow spatial variability

In this study, we compare snow height maps simulated with and without transport using various sources for the precipitation  
485 forcing. The combined impact of precipitation forcing variability and wind-blown redistribution is visible, on snow height, in

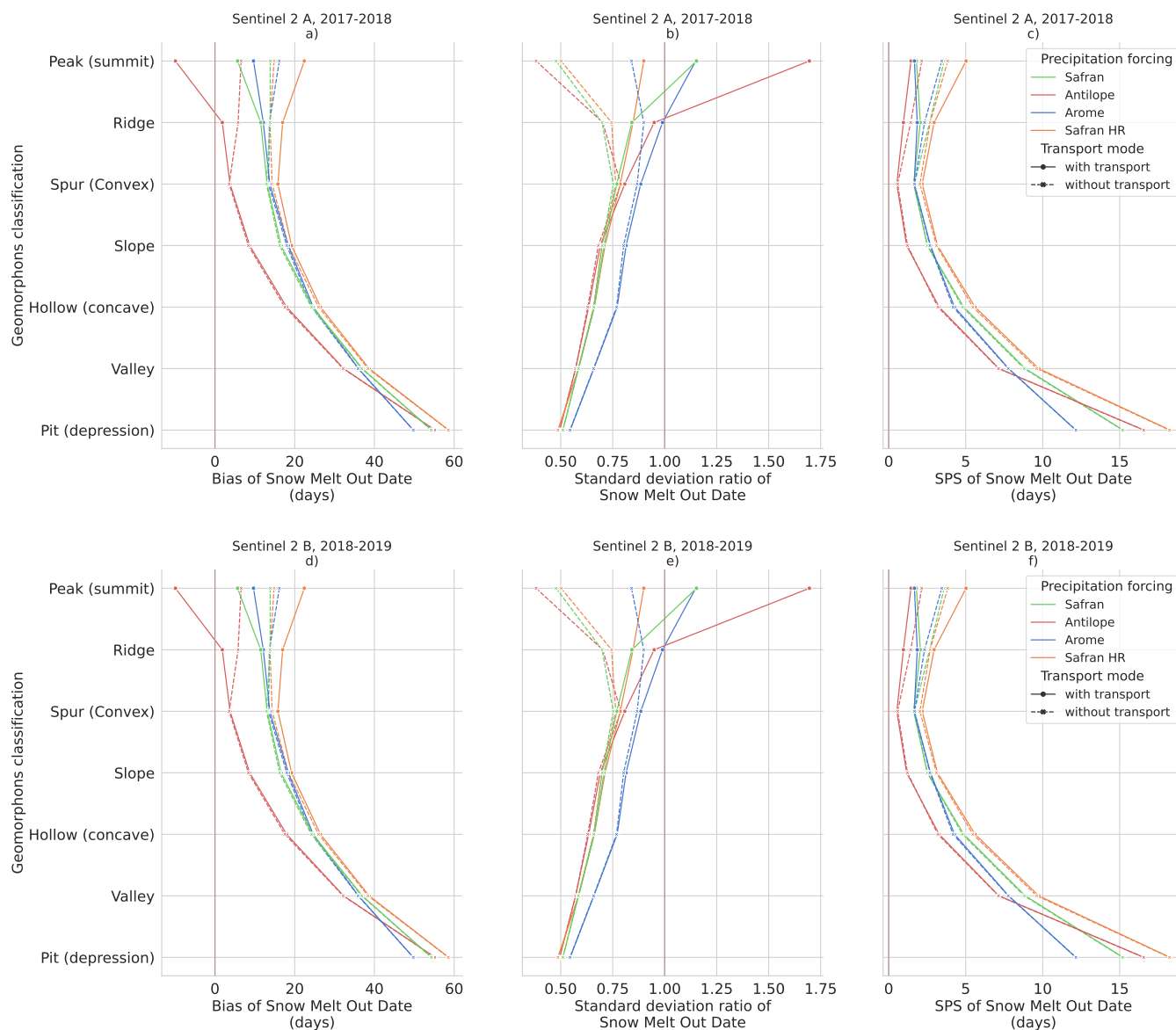


**Figure 12.** Scores comparing simulated SMOD with Sentinel 2 imagery. (a-b-c) 2017-2018 year (Sentinel 2 A) ; (d-e-f) 2018-2019 year (Sentinel 2 B). (a-d) Bias (days) ; (b-e) Standard deviation ratio (no unit) ; (c-f) SPS (days). All scores are presented as a function of landform pixel classification.

Fig. 5 and Fig. 7 and SMOD in Fig. 9. We have found that the main driver of the simulated snow height distribution mean value is the precipitation forcing. The precipitation forcing spatial variability across low to medium altitudes is also found to be the main driver of simulated snow height distribution standard deviation. On the contrary, for the upper altitudes and especially



around summit pixels, the standard deviation of the simulated snow height distribution and the snow melt-out date distribution  
490 is mainly determined by blowing snow transport.

In our simulations, blowing snow transport impact is mostly restricted to 'Peak (summit)' and 'Ridges' landforms and more generally to the upper elevation bands (above 2800 m). In addition, the snow height variance is seen to increase closer to the observation using the simulated snow transport regardless of the precipitation bias. Bernhardt et al. (2012) studied the influence of lateral snow redistribution using SnowTran-3D (Liston et al., 2007) and found an enhancement in the simulated  
495 snow spatial pattern using lateral snow redistribution. Using the Canadian Hydrological Model (Marsh et al., 2020), Vionnet et al. (2021) find snowpack simulation without lateral snow redistribution unable to capture the spatial variability of snow cover in alpine terrain. The addition of lateral snow redistribution is found to provide the best estimate of snow height across elevation and increase the simulated snow height distribution variance. Very recently, Quéno et al. (2023) evaluated FSM2trans snow redistribution model (Quéno et al., 2023) and find the addition of snow redistribution necessary at hectometric or finer  
500 resolution to better represent snowpack heterogeneity. Snow heights simulated using lateral snow redistribution are found to have significantly better variability. Additionally, (Quéno et al., 2023) conducted a model sensibility analysis to horizontal resolution and found that although the most realistic simulation pattern was found at 25 m resolution, the addition of lateral snow redistribution at coarser resolution is found also having a positive impact on snow distribution and variance. Hence, we estimate that the results obtained in this study on the impact of snow transport are compatible with the results found in the  
505 literature.

In this study, we tested the sensitivity of the spatial snow height variability found in our simulation to the variability of precipitation, snow transport, and spatial resolution, but numerous other processes shape snow spatial variability in the field (as reviewed in Mott et al. (2018)). Those processes occur at different scales, going from the regional scale to the slope and lower scale. It is worth noticing that neither preferential deposition nor the seeder-feeder mechanism is represented in our  
510 simulations. Looking at the Pleiades bias values in Fig. 6 and Fig. 8 (a) and (d), blowing snow reduces the absolute mean bias value of snow height in all simulations. This is probably a combined effect of increased snow density and mass loss from increased sublimation. This result is consistent with Vionnet et al. (2021). In a simulation with a precipitation dataset leading to an already negatively biased snow height (ANTILOPE), the addition of snow transport further degrades the overall snow height simulation bias. Similar behavior is found on the SMOD in Fig. 10 (a) and (d) with an exception for the 30m simulation  
515 where it increases the absolute SMOD bias. Thus the beneficial or detrimental impact of blowing snow transport on mean snow height or SMOD bias is mainly dependent on the precipitation bias. This result is consistent with Raleigh et al. (2015); Schögl et al. (2016); Günther et al. (2019), also finding the prevalence of meteorological forcing errors in snow simulations.

## 4.2 On the precipitation forcings

As the Crocus snow model is known to produce realistic snow heights and snow water equivalent when forced by well-  
520 controlled meteorological forcing (Lafaysse et al., 2017; Menard et al., 2021), the large biases of snow height and SMOD obtained in the simulations presented in this paper probably largely reflect intrinsic biases of the different precipitation dataset. More specifically, when looking at the simulation forcing with the ANTILOPE precipitation source, we found that across



all elevation bands, the ANTILOPE forcings have the lowest snow height and SMOD values. Furthermore, a negative bias trend is seen with elevation. The ANTILOPE product is primarily based on radar reflectivity measurements, known to be  
525 more challenging in mountainous terrains (Yu et al., 2018; Faure et al., 2019; Foresti et al., 2018; Germann et al., 2022). Meteorological radars are based on the backscatter measurement of several conic-shaped microwave electromagnetic impulses produced by the radar itself at several elevation angles (conic-shaped radar beams). When a mountain intercepts a radar beam, the reflected signal (called ground clutter) is unusable and rejected by the ANTILOPE algorithm. If the mountain intercepts less than 70% of the beam section, the signal reflected further away is simply corrected to account for the loss of information but  
530 is still used for precipitation rate estimation. Precipitation estimation over pixels affected by ground clutters thus comes from beams that can be several thousands of meters higher than the mountain, often above the base of precipitation clouds. This leads to an underestimation of the precipitation rate over mountain ridges (Appendix Fig. B1), due to ground clutter. One possible compromise would consist of using the observed spatial variability from ANTILOPE while correcting the elevation-dependent precipitation bias.

535 In contrast to ANTILOPE, our simulations with the AROME precipitation source lead, on average, to the highest snow height across the elevation bands. It is particularly visible in Fig. 4 (b), where the snow height patterns come from the 1.3km AROME pixels, forming distinctive precipitation patterns (see Appendix Fig. B1 (d)). This behavior of excessive solid precipitation at high elevations is known and coherent with other snow cover studies using AROME as the precipitation source (Quéno et al., 2016; Vionnet et al., 2019; Monteiro et al., 2022). Multifactorial causes were discussed by Monteiro et al. (2022); Gouttevin  
540 et al. (2023). The variable biases between the western (Grandes Rousses) and eastern (Galibier) evaluation areas suggest that orographic enhancement of precipitation might be especially overestimated by AROME on the areas the most exposed to the prevailing westerly flows.

In contrast, the two SAFRAN simulations that are the only ones to assimilate precipitation gauge observations show a good agreement in terms of SMOD and snow height biases but are spatially under-dispersed by design. The SAFRAN meteorological  
545 reanalysis (Vernay et al., 2022) uses one vertical profile per climatologically homogeneous area, interpolated to all simulation points with altitude (see Sect. 2.5.1). Within one of these areas, the spatial variability is thus limited to a vertical gradient as described in Vionnet et al. (2016). This also explains why opposite snow height biases are obtained with this forcing between western (Grandes Rousses) and eastern (Galibier) areas.

### 4.3 Limitations of the study

550 This study highlights the difficulties in disentangling precipitation and blowing snow errors in snow simulation. Our results show that precipitation forcing is the largest contributor to snow height error across elevation. The utmost care must be taken to estimate the precipitation field as accurately as possible. Our numerical simulations naturally have other types of errors and limitations.



### 4.3.1 Sensitivity to horizontal resolution

555 Numerical simulations rely on numerical discretization and parameterization. The choice of the spatial resolution introduces errors. This choice depends on a trade-off between scientific arguments, computing resources, and external factors. As described in Baron et al. (2023), the 250 m resolution choice of the SnowPappus scheme was motivated by the desire for applicability in large-extent systems (50000 to 100000 km<sup>2</sup>, multi-decadal simulations). Numerical resolution choices impact simulated slope inclinations and aspects and can lead to inaccuracy in the radiative balance (Baba et al., 2019). The snow radiative balance is particularly heterogeneous in mountainous areas due to complex topography leading to significant changes in snow properties and melting rates. Comparing simulations computed at 250 and 30 m resolution provides an analysis of the unresolved subgrid variability of our simulations. Direct comparison between Appendix Fig. C1 (a-b-c) illustrates the expected unresolved subgrid variability. Snow height patterns on the 250 m simulations (Appendix Fig. C1(a)) exhibit steeper variations than the 250 m re-gridded maps obtained from 30 m simulations (Appendix Fig. C1 (b)) where the snow patterns are found smoother. To understand the origin of this subgrid variability, Appendix Fig. C1 (c) illustrates the raw 30 m simulation where snow patterns are more sophisticated. As expected (Baba et al., 2019), resolving the 30 m topography in simulation without snow transport increases the spatial variance at high elevations and reduces the 250 m averaged snow height (Sect. 3.1.4). On the other hand, increasing resolution in simulation with snow transport increases the SMOD (Sect. 3.2.4) but reduces the expected snow height variability gain compared to 250 m simulations. Until now, the resolution-dependence of snow transport models was only documented at higher resolutions (Grünewald et al., 2013; Marsh et al., 2020; Mott et al., 2010; Schneiderbauer and Prokop, 2011) but results recently submitted suggest that the resolution-sensitivity of SnowPappus in this range of spatial scales is similar to what is obtained from another snow transport model at similar resolutions (Quéno et al., 2023).

Quéno et al. (2016); Bellaire et al. (2014); Schirmer and Jamieson (2015) also emphasize the relationship between the available resolution of the atmospheric forcing and the resulting snow simulation leading to the recommendation of forcing spatial resolution of 1 km or less, although evaluations of these data are very challenging at this scale. A much lower resolution is needed to capture the relationship between topography wind field and snow accumulation (Dadic et al., 2010) or for a complete representation of wind-driven processes (Mott et al., 2008, 2014; Bernhardt et al., 2010; Vionnet et al., 2017).

Additional errors in snow-wind interaction come from process modeling. In our simulation, only the blowing snow is represented, the preferential deposition and snowfall enhancement are not represented. Blowing snow transport parameterization also suffers from uncertainties. The parameterizations used in our model were developed for flat areas and the question remains on using them in complex turbulent mountain topography. As discussed by Aksamit and Pomeroy (2018), turbulence gust wind, and eddies are some of the main small-scale contributors to blowing snow. In any case, the DEVINE downscaled wind does not yet take into account wind turbulence and recirculation zone. Furthermore, further studies are needed to quantify the relative impact of recirculation zones over lee deceleration at the 250 m spatial resolution used in this work.

585 In our simulations, not all cover types and processes are represented. Forests and glaciers are masked out. When comparing simulations to observations, bias on the border of masked areas likely occurs due to unrealistic snow interactions simulated at the borders of such masked areas. Soil properties are also an important parameter influencing snowpack simulations but they



are often overlooked. Our simulations use the 1km resolution ECOCLIMAP landcover database (Champeaux et al., 2005) and the 1km Harmonized World Soil Database (HWSD) v1.10 (Nachtergaele et al., 2009) as the reference for soil properties. The spatial variability of soil properties in mountains is significant and the 1km resolution of the HWSD database might not capture enough of the spatial variability, leading to spatial errors.

#### 4.3.2 Uncertainties and limitations of observations

In this work, simulations are evaluated against spatialized snow observations, giving a larger perspective than point snow observations. Indeed, although point scale snow observations are commonly used to evaluate spatialized simulations (Horton and Haegeli, 2022; Vernay et al., 2022; Vionnet et al., 2022; Mott et al., 2023; Marsh et al., 2020), their spatial distribution and representativeness is quite low in mountains (Grünewald and Lehning, 2015; Pomeroy et al., 2009; Pepin et al., 2015), while satellite snow observations like Pleiades snow height and Sentinel 2 SMOD have a much better spatial coverage and representativeness. Nonetheless, some errors and limitations also come from the observation side. The Pleiades observations are on-demand snapshots of snow height over a predefined extent and at a specific date. By design, this limits the usage of Pleiades images and the extent to which our conclusions stay valid. Pleiades observations of snow height can be affected by shadows, steep slopes, and the reference image used in the processing method. These limitations restrict the domain of observations and make it difficult to retrieve accurate snow height on glaciers. The Pleiades horizontal resolution of 2 m causes challenges in comparison with coarser resolution simulation. Unsimulated sub-grid processes are captured by the observation, which complexifies the analysis. For the Sentinel 2 observations, the major limitation comes from the snow detection algorithm. The presence or absence of snow is not directly comparable to our simulation output. In Sect. 2.8.1, the presence or absence of snow is expressed as a function based on a given simulated snow height threshold. This raises the question of the sensitivity to this threshold (Gascoïn et al., 2019; Hofmeister et al., 2022).

#### 4.3.3 Impact of the grid cells classification in spatial evaluations

Classically in the snow modeling community, the quantitative spatial snow evaluations are performed by grouping simulation points (Grünewald et al., 2014; Vionnet et al., 2022; Monteiro et al., 2022; Tong et al., 2009; Deschamps-Berger et al., 2022; Vionnet et al., 2017) because (1) it allows to summarize large simulations dataset with more concise diagnostics and (2) these evaluations are less demanding for models than pixel-to-pixel evaluations. In Sect. 3.3, results are presented using landform classification instead of elevation bands. The results are partly correlated because summits and ridges mainly cover the highest elevations of the domain (Fig. 3). Thus, we consistently obtain that snow transport mainly affects snow height and SMOD on the upper elevation bands and on geomorphons 'Peaks (summit)' and 'Ridge'. However, some conclusions significantly differ between both space classifications, especially for the  $\sigma$  ratio score. Using landform grouping, the intra-class variance includes a relatively large spatial variability due to elevation while using elevation grouping, the intra-class variance includes a relatively large spatial variability due to topographic features. This might suggest that these simulations better capture the altitudinal variability of precipitation than their topographic-dependent variability. This result clearly illustrates the sensitivity of some scores to the choice of the grid cell classification.



For the SPS score, a notable difference is found for the snow height comparison. SPS scores are found more homogeneous and smaller using landforms grouping than elevation bands (Fig. 11, Fig. D1 (c-f)). This suggests simulated and observed distributions are closer when grouped using landforms than elevation bands. Thus for Grandes Rousses and Galibier areas, we can again conclude that the observed snow height variability due to elevation is better captured than the variability due to  
625 landform.

The landform classification also provides complementary insights into the behavior of the SnowPappus model. In Fig. 11 and Fig. D1 (a-d), SnowPappus reduces the mean snow height on pixels classified as 'Peak (summit)' and 'Ridges' and increases the snow height on 'Spur (convex)', 'Slope' and 'Hollow (concave)' comparatively to simulations without snow transport. This behavior is the result of the wind spatial patterns obtained from Le Toumelin et al. (2023). It can be understood as snow on  
630 'Peak (summit)' and 'Ridges' (ablation areas) being transported to pixels classified as 'Spur (convex)', 'Slope' or 'Hollow (concave)' (deposition areas) due to respective wind acceleration and deceleration on these pixels. This behaviour is similar between all 250 m resolution simulations while different patterns are obtained from the 30m SAFRAN HR simulation. Indeed, the finer spatial scales resolved at 30-m resolution produce more complex spatial patterns of wind fields and snow transport. When averaged at 250-m resolution, these simulations produce a more subtle influence of snow transport than simulations at  
635 the coarser 250-m resolution, with a less direct influence of the 250-m topography on the simulated snow patterns.

## 5 Conclusions

We conducted a spatialized evaluation of the blowing snow model SnowPappus (Baron et al., 2023) joint with a sensitivity analysis to alpine precipitation variability on a 902 km<sup>2</sup> area representative of the French Alps and the Pyrenees in terms of landforms. We evaluated the simulated snow height and Snow Melt Out Date (SMOD) using Pleiades and Sentinel 2  
640 satellite products. The Pleiades comparisons were conducted in two different areas, for different times in the same snow season and in between two snow seasons. Eight different snow simulations have been run over three snow seasons with three different precipitation forcings and two simulation resolutions (Table 1). We performed simulation analysis with the aim of disentangling simulation error contributions between the SnowPappus blowing snow model, precipitation forcings, and the unresolved subgrid variability. The main conclusions of this study are :

- 645 – Simulations without snow transport are found unable to capture the spatial variability of snow cover in alpine terrain. The addition of snow transport to simulations provides a better estimate of snow height across elevations and increases the simulated snow height variance regardless of the precipitation forcing bias.
- Precipitation errors overlook the bias and the standard deviation of snow height and SMOD at low to medium altitudes. This result underlines that the greatest care must be taken to obtain the most accurate precipitation fields for snow  
650 simulation. It also suggests that assessments of spatial snow simulations that do not account for precipitation uncertainty are unlikely to provide informative insights regarding the accuracy of particular simulated snow processes.



- Blowing snow transport impact on snow height, SMOD bias, and standard deviation prevail for high altitudes or pixels classified by the landform classifier as 'Peak (summit)' and 'Ridges'.
- Simulated snow heights are found relatively close between the two computation resolutions (250 m, 30 m) in terms of snow height bias,  $\sigma$  ratio, and SPS values. Changes in spatial variance and bias when increasing resolution from 250 m to 30 m are lower than the simulated spatial variability due to precipitation inputs and the impact of blowing snow in the proper affected areas.
- The addition of the SnowPappus blowing snow model to a 250 m Crocus snowpack simulation always increases and improves the simulated snow spatial variability at high elevations in accordance with observations. However, improvement of snow height and SMOD biases are only obtained using precipitation forcing that does not suffer from strong negative biases.

The findings of this study show promising results of using the SnowPappus blowing snow model for large-scale modeling of alpine snowpack. Future work will focus on adding to the simulation workflow assimilation methods to improve precipitation estimates. Our results suggest that snow transport impact on snow height at 250 m resolution is significant at high elevations and therefore needs to be accounted for. However, unresolved processes at this spatial scale, parameterization uncertainty, and evaluation challenges are responsible for large uncertainties that will need to be appropriately quantified in future works, especially with the goal of designing a snow ensemble assimilation frameworks (e.g. Cluzet et al., 2021; Deschamps-Berger et al., 2022).

*Code and data availability.* The SnowPappus blowing snow model is developed in the framework of the open-source SURFEX project. The source files of the SURFEX system (Crocus snow model, ISBA ground model, and SnowPappus model) are provided at <https://doi.org/10.5281/zenodo.7687821> to guarantee the permanent reproducibility of results. However, we recommend that potential future users and developers access the code from its Git repository to benefit from all tools of code management (history management, bug fixes, documentation, interface for technical support, etc.). This requires a free and quick registration. The procedure is described at [https://opensource.umr-cnrm.fr/projects/snowtools\\_git/wiki/Install\\_SURFEX](https://opensource.umr-cnrm.fr/projects/snowtools_git/wiki/Install_SURFEX). The version used in this work is tagged as SnowPappus-v1.0. A user manual, describing the SURFEX namelist options related to SnowPappus is available at <https://doi.org/10.5281/zenodo.7681340>. More general information about SURFEX use can be found at [https://opensource.umr-cnrm.fr/projects/snowtools\\_git/wiki](https://opensource.umr-cnrm.fr/projects/snowtools_git/wiki).

The code and model weights used for DEVINE are available freely at [https://github.com/louisletoumelin/neural\\_network\\_and\\_devine/](https://github.com/louisletoumelin/neural_network_and_devine/).

The WhiteboxTools Open Core software used to compute the landforms classification is freely available at <https://www.whiteboxgeo.com/>.

The Earth System Modeling Framework (ESMF) software is freely available at <https://earthsystemmodeling.org/>.

The GDAL software is also freely available <https://doi.org/10.5281/zenodo.8340595>.

The DEM used in this study originates from IGN® website. Tiles can be downloaded freely at <https://geoservices.ign.fr/rgealti>.

Forest mask originates from IGN® and can be downloaded freely at <https://geoservices.ign.fr/bdforet>.

Waterways, lakes, and cities' spatial extent originate from IGN® and can be downloaded freely at <https://geoservices.ign.fr/bdforet>.

The glacier masks can be downloaded freely from the Randolph glacier inventory at <http://glims.colorado.edu/glacierdata/>.



- 685 The SAFRAN reanalysis dataset is freely available on the AERIS data center on the following link <https://doi.org/10.25326/37#v2020.2>.  
The AROME and ANTILOPE precipitation dataset can be requested online <https://donneespubliques.meteofrance.fr/>.  
The Sentinel 2 Level 3 dataset can be accessed at <https://www.theia-land.fr/en/product/snow/>.  
The raw Pleiades images are not publicly available. The 250 m averaged Pleiades images can be found at <https://doi.org/10.5281/zenodo.10037253>.
- 690 (The data accessibility and URL links status is confirmed on 24 Oct 2023)

*Author contributions.* A.H. ran the simulations, collected and processed the different data, wrote the paper, and made the spatial evaluations and the scientific choices. A.H. and M.B. developed jointly the SnowPappus code with equal contribution. M.B. helped write the Crocus and SnowPappus sections. M.L. supervised the work, helped a lot with the scientific choices, and provided technical support on Crocus and SURFEX. M.L. and M.D. were extensively involved in the proofreading process and the scientific choices. L.LT provided the DEVINE  
695 downscaled wind forcing and helped in writing the wind DEVINE section. M.V. provided the ANTILOPE precipitation forcing and helped the writing of the ANTILOPE section. C.D.B. and S.G. provided the Pleiades images and the stereo-imagery treatment. C.D.B., S.G., and V.V. helped with the evaluation methodology, participated in theoretical discussions, and proofread the article.

*Competing interests.* One of the co-authors is a member of the editorial board of The Cryosphere. Other authors have no competing interests to declare.

700 *Acknowledgements.* This investigation was done using Meteo France's CNRM's, and CEN's computational and human resources. CNRM/-CEN is part of LabEx OSUG@2020. The main source of funding is the Region Auvergne Rhône-Alpes (France) SENSASS project and CNES TOSCA. We gratefully acknowledge Sabine Radanovics, Diego Monteiro, and Matthieu Fructus for their expertise.



## Appendix A: Additional domain characteristics

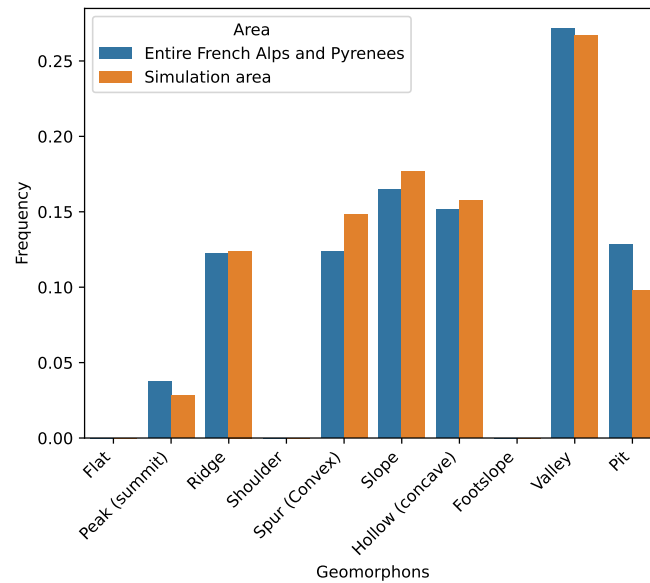


**Figure A1.** Landforms classification frequency (at 250 m) for our simulation domain and the entire French Alps and Pyrenees (as an area defined in Vernay et al. (2022)). We found a good agreement between our simulation pixel classification and the frequency of the French Alps and Pyrenees. We note that using 250 m resolution, no pixel corresponding to shoulder, footslope, and flat are classified as such.



### Appendix B: Additional map of mean daily precipitation variability

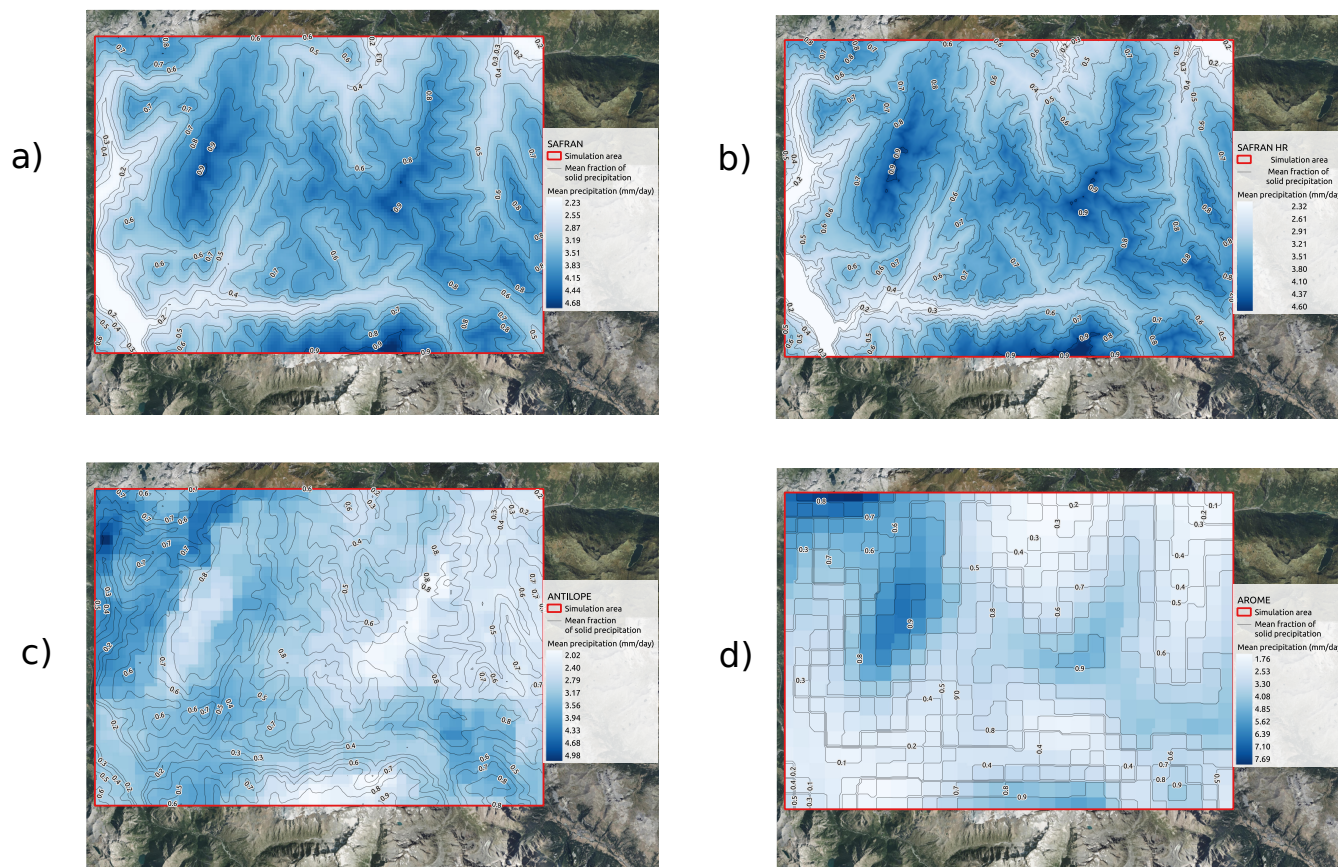


**Figure B1.** Map of the mean daily precipitation over 2017-2020 in (mm/day) for the 4 different forcings. This illustrates the spatial variability of each precipitation dataset (a. SAFRAN, b. SAFRAN HR, c. ANTILOPE, d. AROME). In each map, the mean solid fraction of precipitation is displayed as a contour plot (i.e. 1=only solid precipitation). The summer aerial photography base map is from IGN© (2022).



705 **Appendix C: Additional map of simulated snow height for Pleiades 1, 13 May 2019**

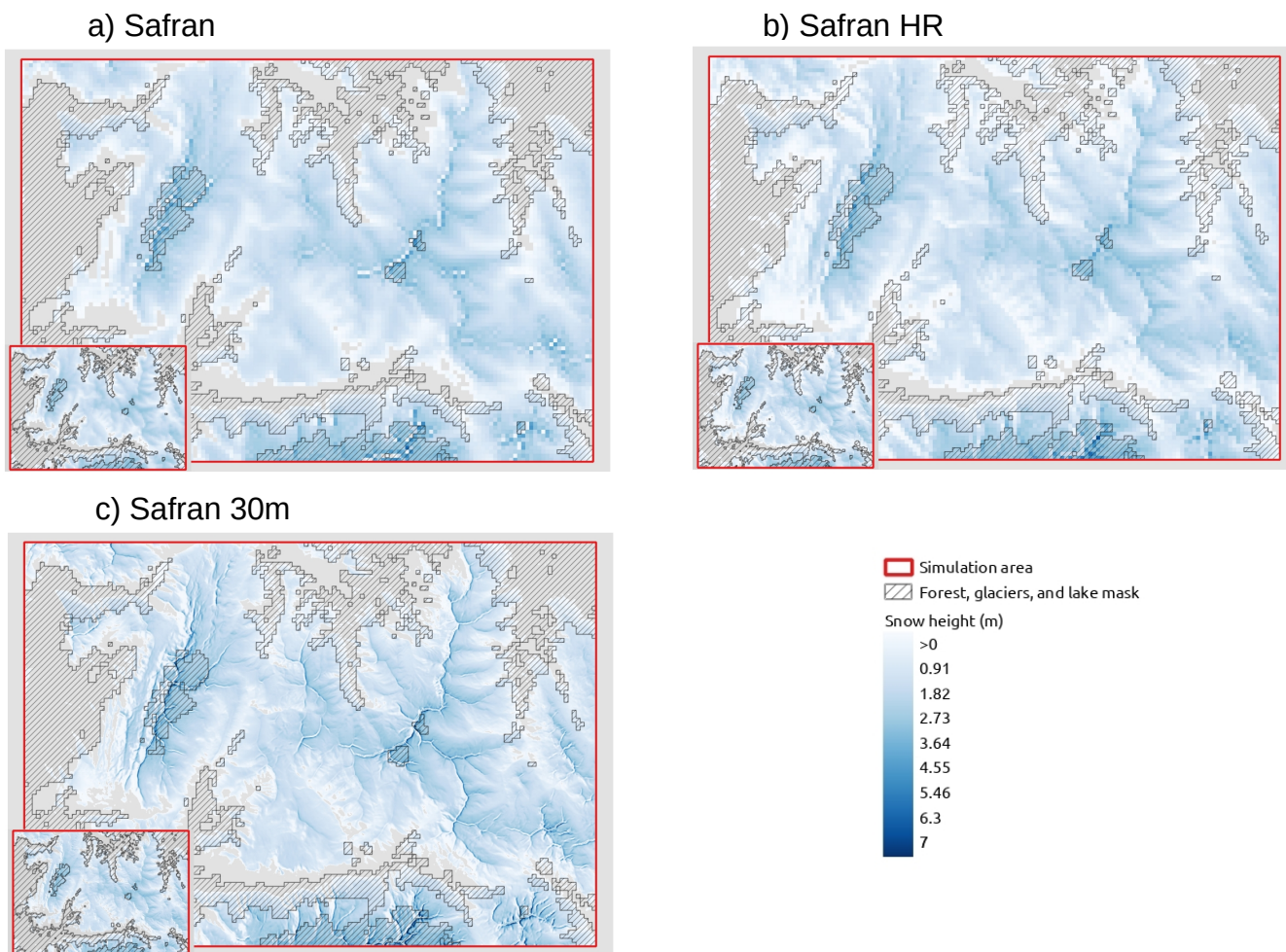


**Figure C1.** Map of simulated snow height on the 13 May 2019 10:00. (a) Safran 250m simulation with snow transport and without snow transport in the left submap. (b) Safran HR simulation (30 m computed resampled to 250m) with snow transport and without snow transport in the left submap. (c) Raw Safran 30m simulation with snow transport and without snow transport in the left submap. The absence of snow is indicated in grey.



## Appendix D: Additional landform analysis

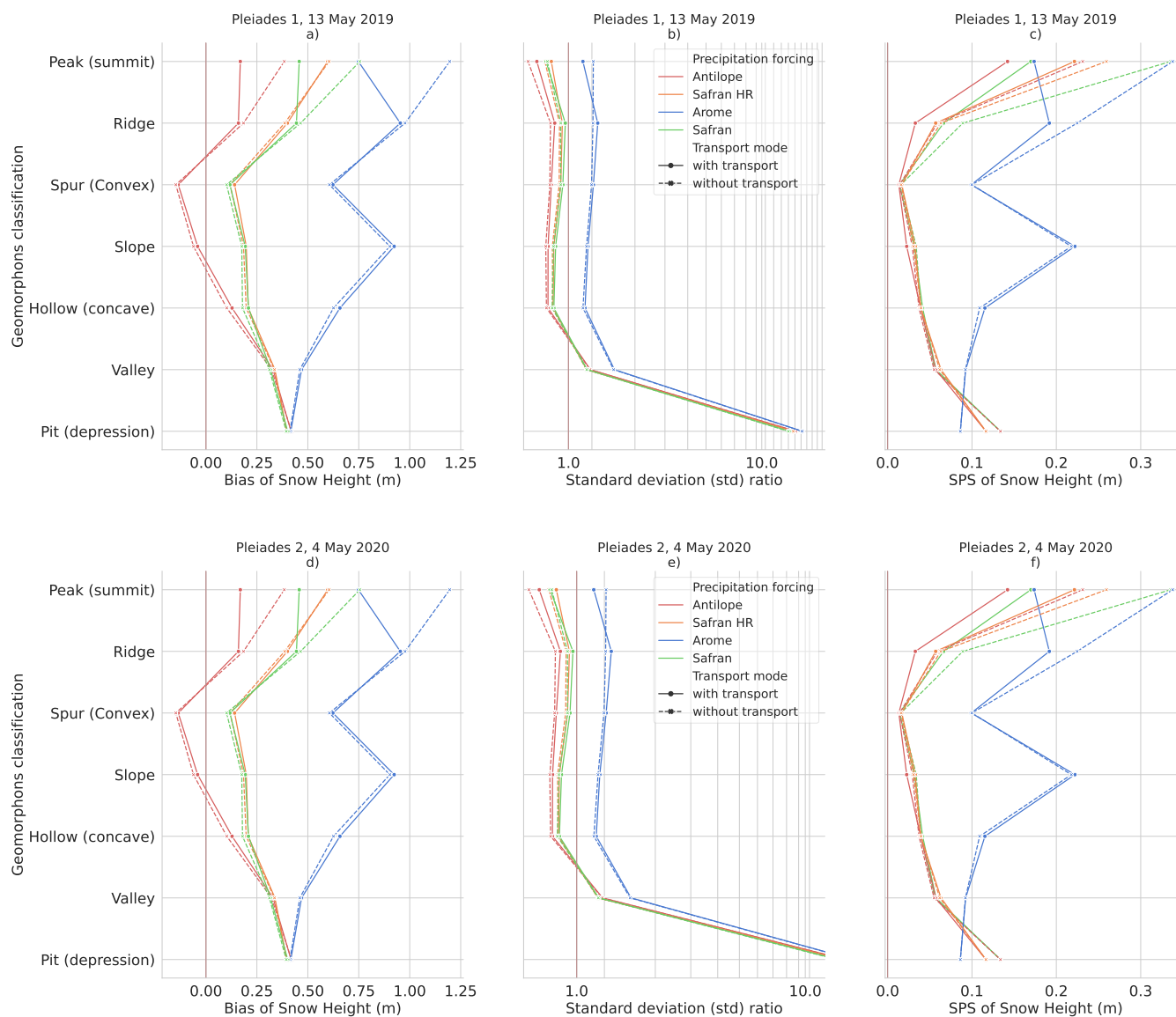


**Figure D1.** Scores comparing simulations with the Grandes Rousses Pleiades observations. (a-b-c) compares simulations with the 13 May 2019 Pleiades 1 image ; (d-e-f) is based on the 4 May 2020 Pleiades 2 image. (a-d) Bias (m) ; (b-e)  $\sigma$  ratio (no unit) ; (c-f) SPS. The important standard deviation ratio values found for the 'Pit' landform type in (b) and (e) are explained because almost all pixels of this type have no observed snow whereas the simulations give snow on every pixel. This is particularly visible in Subfigure (d) and (e) where Antilope, Safran, and Safran HR have almost no simulated snow and a fair standard deviation ratio but Antilope. All scores are presented as a function of landform pixel classification.



## References

- Aksamit, N. O. and Pomeroy, J. W.: Scale Interactions in Turbulence for Mountain Blowing Snow, *Journal of Hydrometeorology*, 19, 305 – 320, <https://doi.org/https://doi.org/10.1175/JHM-D-17-0179.1>, 2018.
- 710 Amory, C., Kittel, C., Le Toumelin, L., Agosta, C., Delhasse, A., Favier, V., and Fettweis, X.: Performance of MAR (v3.11) in simulating the drifting-snow climate and surface mass balance of Adélie Land, East Antarctica, *Geoscientific Model Development*, 14, 3487–3510, <https://doi.org/10.5194/gmd-14-3487-2021>, 2021.
- Anderson, B. T., McNamara, J. P., Marshall, H.-P., and Flores, A. N.: Insights into the physical processes controlling correlations between snow distribution and terrain properties, *Water Resources Research*, 50, 4545–4563, <https://doi.org/https://doi.org/10.1002/2013WR013714>, 2014.
- 715 Baba, M. W., Gascoïn, S., Kinnard, C., Marchane, A., and Hanich, L.: Effect of Digital Elevation Model Resolution on the Simulation of the Snow Cover Evolution in the High Atlas, *Water Resour. Res.*, 55, 5360–5378, <https://doi.org/10.1029/2018WR023789>, 2019.
- Bales, R. C., Molotch, N. P., Painter, T. H., Dettinger, M. D., Rice, R., and Dozier, J.: Mountain hydrology of the western United States, *Water Resources Research*, 42, <https://doi.org/10.1029/2005WR004387>, 2006.
- 720 Baron, M., Haddjeri, A., Lafaysse, M., Le Toumelin, L., Vionnet, V., and Fructus, M.: SnowPappus v1.0, a blowing-snow model for large-scale applications of Crocus snow scheme, *Geoscientific Model Development Discussions*, 2023, 1–52, <https://doi.org/10.5194/gmd-2023-43>, 2023.
- Bellaire, S., Katurji, M., Schulmann, T., and Hobman, A.: Towards a high-resolution operational forecasting tool for the southern alps - New Zealand, in: *roceedings, International Snow Science Workshop, Banff, 2014, 2014*.
- 725 Bergeron, T.: On the low-level redistribution of atmospheric water caused by orography, in: *Proc. of the Int. Conf. on Cloud Physics*, pp. 96–100, 1965.
- Bernhardt, M. and Schulz, K.: SnowSlide: A simple routine for calculating gravitational snow transport, *Geophysical Research Letters*, 37, 2010.
- Bernhardt, M., Liston, G. E., Strasser, U., Zängl, G., and Schulz, K.: High resolution modelling of snow transport in complex terrain using downscaled MM5 wind fields, *The Cryosphere*, 4, 99–113, <https://doi.org/10.5194/tc-4-99-2010>, 2010.
- 730 Bernhardt, M., Schulz, K., Liston, G. E., and Zängl, G.: The influence of lateral snow redistribution processes on snow melt and sublimation in alpine regions, *Journal of Hydrology*, 424–425, 196–206, <https://doi.org/10.1016/j.jhydrol.2012.01.001>, 2012.
- Brauchli, T., Trujillo, E., Huwald, H., and Lehning, M.: Influence of slope-scale snowmelt on catchment response simulated with the Alpine3D model, *Water Resources Research*, 53, 10723–10739, 2017.
- 735 Brun, E., Martin, E., Simon, V., Gendre, C., and Coleou, C.: An Energy and Mass Model of Snow Cover Suitable for Operational Avalanche Forecasting, *Journal of Glaciology*, 35, 333–342, <https://doi.org/10.3189/S0022143000009254>, 1989.
- Candille, G. and Talagrand, O.: Evaluation of probabilistic prediction systems for a scalar variable, *Quart. J. Roy. Meteorol. Soc.*, 131, 2131–2150, <https://doi.org/10.1256/qj.04.71>, 2005.
- Champeaux, J. L., Masson, V., and Chauvin, F.: ECOCLIMAP: a global database of land surface parameters at 1 km resolution, *Meteorological Applications: A journal of forecasting, practical applications, training techniques and modelling*, 12, 29–32, 2005.
- 740 Champeaux, J.-L., Dupuy, P., Laurantin, O., Soulan, I., Tabary, P., and Soubeyroux, J.-M.: Les mesures de précipitations et l'estimation des lames d'eau à Météo-France : état de l'art et perspectives, *La Houille Blanche*, 95, 28–34, <https://doi.org/10.1051/lhb/2009052>, 2009.



- Choularton, T. W. and Perry, S. J.: A model of the orographic enhancement of snowfall by the seeder-feeder mechanism, *Quarterly Journal of the Royal Meteorological Society*, 112, 335–345, <https://doi.org/10.1002/qj.49711247204>, 1986.
- 745 Clark, M. P., Hendriks, J., Slater, A. G., Kavetski, D., Anderson, B., Cullen, N. J., Kerr, T., Hreinsson, E. Ö., and Woods, R. A.: Representing spatial variability of snow water equivalent in hydrologic and land-surface models: A review, *Water Resour. Res.*, 47, W07539, <https://doi.org/10.1029/2011WR010745>, 2011.
- Cluzet, B., Lafaysse, M., Cosme, E., Albergel, C., Meunier, L.-F., and Dumont, M.: CrocO\_v1.0: a particle filter to assimilate snowpack observations in a spatialised framework, *Geosci. Model Dev.*, 14, 1595–1614, <https://doi.org/10.5194/gmd-14-1595-2021>, 2021.
- 750 Colle, B. A., Smith, R. B., and Wesley, D. A.: Theory, observations, and predictions of orographic precipitation, *Mountain Weather Research and Forecasting: Recent Progress and Current Challenges*, pp. 291–344, 2013.
- Dadic, R., Mott, R., Lehning, M., and Burlando, P.: Wind influence on snow depth distribution and accumulation over glaciers, *Journal of Geophysical Research: Earth Surface*, 115, <https://doi.org/10.1029/2009JF001261>, 2010.
- Decharme, B., Boone, A., Delire, C., and Noilhan, J.: Local evaluation of the Interaction between Soil Biosphere Atmosphere soil multilayer diffusion scheme using four pedotransfer functions, *J. Geophys. Res.*, 116, D20126, <https://doi.org/10.1029/2011JD016002>, 2011.
- 755 Deschamps-Berger, C., Gascoïn, S., Berthier, E., Deems, J., Gutmann, E., Dehecq, A., Shean, D., and Dumont, M.: Snow depth mapping from stereo satellite imagery in mountainous terrain: evaluation using airborne laser-scanning data, *The Cryosphere*, 14, 2925–2940, 2020.
- Deschamps-Berger, C., Cluzet, B., Dumont, M., Lafaysse, M., Berthier, E., Fanise, P., and Gascoïn, S.: Improving the Spatial Distribution of Snow Cover Simulations by Assimilation of Satellite Stereoscopic Imagery, *Water Resour. Res.*, 58, e2021WR030271, <https://doi.org/10.1029/2021WR030271>, 2022.
- 760 Durand, Y., Brun, E., Mérindol, L., Guyomarc’h, G., Lesaffre, B., and Martin, E.: A meteorological estimation of relevant parameters for snow models, *Ann. Glaciol.*, 18, 65–71, <https://doi.org/10.3189/S0260305500011277>, 1993.
- Earth System Modeling Framework, University Corporation for Atmospheric Research, Massachusetts Institute of Technology, Geophysical Fluid Dynamics Laboratory, University of Michigan, National Centers for Environmental Prediction, Los Alamos National Laboratory, Argonne National Laboratory, and NASA Goddard Space Flight Center: Earth System Modeling Framework (ESMF) Grid Remapping (Version 8.4.2), <https://earthsystemmodeling.org/>, 2023.
- 765 Essery, R., Li, L., and Pomeroy, J.: A distributed model of blowing snow over complex terrain, *Hydrological Processes*, 13, 2423–2438, [https://doi.org/10.1002/\(SICI\)1099-1085\(199910\)13:14/15<2423::AID-HYP853>3.0.CO;2-U](https://doi.org/10.1002/(SICI)1099-1085(199910)13:14/15<2423::AID-HYP853>3.0.CO;2-U), 1999.
- Faure, D.: Quality Analysis of the 2016 Quantitative Precipitation Estimates in the French Alps, in: 37th Conference on radar meteorology, AMS, <https://ams.confex.com/ams/38RADAR/webprogram/Paper320389.html>, 2017.
- 770 Faure, D., Delrieu, G., and Gaussiat, N.: Impact of the Altitudinal Gradients of Precipitation on the Radar QPE Bias in the French Alps, *Atmosphere*, 10, <https://doi.org/10.3390/atmos10060306>, 2019.
- Foresti, L., Sideris, I. V., Panziera, L., Nerini, D., and Germann, U.: A 10-year radar-based analysis of orographic precipitation growth and decay patterns over the Swiss Alpine region, *Quarterly Journal of the Royal Meteorological Society*, 144, 2277–2301, <https://doi.org/https://doi.org/10.1002/qj.3364>, 2018.
- 775 Froidurot, S., Zin, I., Hingray, B., and Gautheron, A.: Sensitivity of precipitation phase over the Swiss Alps to different meteorological variables, *Journal of Hydrometeorology*, 15, 685–696, 2014.
- Gascoïn, S., Grizonnet, M., Bouchet, M., Salgues, G., and Hagolle, O.: Theia Snow collection: high-resolution operational snow cover maps from Sentinel-2 and Landsat-8 data, *Earth Syst. Sci. Data*, 11, 493–514, <https://doi.org/10.5194/essd-11-493-2019>, 2019.



- 780 GDAL/OGR contributors: GDAL/OGR Geospatial Data Abstraction software Library (Version 3.6.2), Open Source Geospatial Foundation, <https://doi.org/10.5281/zenodo.5884351>, 2023.
- Germann, U., Boscacci, M., Clementi, L., Gabella, M., Hering, A., Sartori, M., Sideris, I. V., and Calpini, B.: Weather Radar in Complex Orography, *Remote Sensing*, 14, <https://doi.org/10.3390/rs14030503>, 2022.
- Goessling, H. and Jung, T.: A probabilistic verification score for contours: Methodology and application to Arctic ice-edge forecasts, *Quarterly Journal of the Royal Meteorological Society*, 144, 735–743, 2018.
- 785 Gouttevin, I., Vionnet, V., Seity, Y., Boone, A., Lafaysse, M., Deliot, Y., and Merzisen, H.: To the Origin of a Wintertime Screen-Level Temperature Bias at High Altitude in a Kilometric NWP Model, *J. Hydrometeorol.*, 24, 53 – 71, <https://doi.org/10.1175/JHM-D-21-0200.1>, 2023.
- Grünewald, T., Stötter, J., Pomeroy, J. W., Dadic, R., Moreno Baños, I., Marturià, J., Sproß, M., Hopkinson, C., Burlando, P., and Lehning, M.: Statistical modelling of the snow depth distribution in open alpine terrain, *Hydrology and Earth System Sciences*, 17, 3005–3021, 2013.
- 790 Grünewald, T., Bühler, Y., and Lehning, M.: Elevation dependency of mountain snow depth, *The Cryosphere*, 8, 2381–2394, 2014.
- Grünewald, T. and Lehning, M.: Are flat-field snow depth measurements representative? A comparison of selected index sites with areal snow depth measurements at the small catchment scale, *Hydrological Processes*, 29, 1717–1728, <https://doi.org/10.1002/hyp.10295>, 2015.
- 795 Guyomarc’h, G., Bellot, H., Vionnet, V., Naaim-Bouvet, F., Déliot, Y., Fontaine, F., Puglièse, P., Nishimura, K., Durand, Y., and Naaim, M.: A meteorological and blowing snow data set (2000–2016) from a high-elevation alpine site (Col du Lac Blanc, France, 2720 m a.s.l.), *Earth Syst. Sci. Data*, 11, 57–69, <https://doi.org/10.5194/essd-11-57-2019>, 2019.
- Guyomarc’h, G. and Mérindol, L.: Validation of an application for forecasting blowing snow, *Annals of Glaciology*, 26, 138–143, <https://doi.org/10.3189/1998AoG26-1-138-143>, 1998.
- 800 Günther, D., Marke, T., Essery, R., and Strasser, U.: Uncertainties in Snowpack Simulations—Assessing the Impact of Model Structure, Parameter Choice, and Forcing Data Error on Point-Scale Energy Balance Snow Model Performance, *Water Resour. Res.*, 55, 2779–2800, <https://doi.org/10.1029/2018WR023403>, 2019.
- Hofmeister, F., Arias-Rodriguez, L. F., Premier, V., Marin, C., Notarnicola, C., Disse, M., and Chiogna, G.: Intercomparison of Sentinel-2 and modelled snow cover maps in a high-elevation Alpine catchment, *Journal of Hydrology X*, 15, 100123, <https://doi.org/10.1016/j.hydroa.2022.100123>, 2022.
- 805 Horton, S. and Haegeli, P.: Using snow depth observation to provide insight into the quality of regional-scale snowpack simulations for avalanche forecasting, *EGUsphere*, 2022, 1–28, <https://doi.org/10.5194/egusphere-2022-237>, 2022.
- IGN©: BD Foret@V2, <https://geoservices.ign.fr/bdforet>, 2021a.
- IGN©: BD Topo@, <https://geoservices.ign.fr/bdtopo>, 2021b.
- 810 IGN©: RGE ALTI@5M, <https://geoservices.ign.fr/rgealti>, 2021c.
- IGN©: BD Ortho@, <https://geoservices.ign.fr/bdortho>, 2022.
- IPCC: *The Ocean and Cryosphere in a Changing Climate*, Cambridge University Press, <https://doi.org/10.1017/9781009157964>, 2022.
- Jasiewicz, J. and Stepinski, T. F.: Geomorphons—a pattern recognition approach to classification and mapping of landforms, *Geomorphology*, 182, 147–156, <https://doi.org/10.1016/j.geomorph.2012.11.005>, 2013.
- 815 Lafaysse, M., Cluzet, B., Dumont, M., Lejeune, Y., Vionnet, V., and Morin, S.: A multiphysical ensemble system of numerical snow modelling, *The Cryosphere*, 11, 1173–1198, <https://doi.org/10.5194/tc-11-1173-2017>, 2017.



- Le Toumelin, L., Gouttevin, I., Helbig, N., Galiez, C., Roux, M., and Karbou, F.: Emulating the adaptation of wind fields to complex terrain with deep-learning, *Artif. Intell. Earth Syst.*, pp. 1 – 39, <https://doi.org/10.1175/AIES-D-22-0034.1>, 2022.
- Le Toumelin, L., Gouttevin, I., Galiez, C., and Helbig, N.: A two-folds deep learning strategy to correct and downscale winds over mountains, *Nonlinear Processes in Geophysics Discussions*, 2023, 1–32, 2023.
- 820 Lehning, M., Völksch, I., Gustafsson, D., Nguyen, T. A., Stähli, M., and Zappa, M.: ALPINE3D: a detailed model of mountain surface processes and its application to snow hydrology, *Hydrological Processes: An International Journal*, 20, 2111–2128, 2006.
- Lehning, M., Löwe, H., Ryser, M., and Raderschall, N.: Inhomogeneous precipitation distribution and snow transport in steep terrain, *Water Resources Research*, 44, 2008.
- 825 Lindsay, J.: The whitebox geospatial analysis tools project and open-access GIS, in: *Proceedings of the GIS Research UK 22nd Annual Conference*, The University of Glasgow, pp. 16–18, [https://www.gla.ac.uk/media/Media\\_401757\\_smxx.pdf](https://www.gla.ac.uk/media/Media_401757_smxx.pdf), 2014.
- Liston, G. and Sturm, M.: A snow-transport model for complex terrain, *J. Glaciol.*, 44, 498–516, <https://doi.org/10.3189/S0022143000002021>, 1998.
- Liston, G. E., Haehnel, R. B., Sturm, M., Hiemstra, C. A., Berezovskaya, S., and Tabler, R. D.: Simulating complex snow distributions in windy environments using SnowTran-3D, *J. Glaciol.*, 53, 241–256, <https://doi.org/10.3189/172756507782202865>, 2007.
- 830 Lundquist, J., Hughes, M., Gutmann, E., and Kapnick, S.: Our Skill in Modeling Mountain Rain and Snow is Bypassing the Skill of Our Observational Networks, *Bulletin of the American Meteorological Society*, 100, 2473–2490, <https://doi.org/10.1175/BAMS-D-19-0001.1>, 2019.
- Marsh, C. B., Pomeroy, J. W., and Wheeler, H. S.: The Canadian Hydrological Model (CHM) v1.0: a multi-scale, multi-extent, variable-complexity hydrological model – design and overview, *Geosci. Model Dev.*, 13, 225–247, <https://doi.org/10.5194/gmd-13-225-2020>, 2020.
- 835 Marsh, C. B., Vionnet, V., and Pomeroy, J. W.: Windmapper: An Efficient Wind Downscaling Method for Hydrological Models, *Water Resources Research*, 59, e2022WR032683, <https://doi.org/10.1029/2022WR032683>, 2023.
- Marti, R., Gascoïn, S., Berthier, E., de Pinel, M., Houet, T., and Laffly, D.: Mapping snow depth in open alpine terrain from stereo satellite imagery, *The Cryosphere*, 10, 1361–1380, <https://doi.org/10.5194/tc-10-1361-2016>, 2016.
- 840 Masson, V., Le Moigne, P., Martin, E., Faroux, S., Alias, A., Alkama, R., Belamari, S., Barbu, A., Boone, A., Bouysse, F., Brousseau, P., Brun, E., Calvet, J.-C., Carrer, D., Decharme, B., Delire, C., Donier, S., Essaouini, K., Gibelin, A.-L., Giordani, H., Habets, F., Jidane, M., Kerdraon, G., Kourzeneva, E., Lafaysse, M., Lafont, S., Lebeaupin Brossier, C., Lemonsu, A., Mahfouf, J.-F., Marguinaud, P., Mokhtari, M., Morin, S., Pigeon, G., Salgado, R., Seity, Y., Taillefer, F., Tanguy, G., Tulet, P., Vincendon, B., Vionnet, V., and Voltaire, A.: The SURFEXv7.2 land and ocean surface platform for coupled or offline simulation of Earth surface variables and fluxes, *Geosci. Model Dev.*, 6, 929–960, <https://doi.org/10.5194/gmd-6-929-2013>, 2013.
- 845 Ménard, C. B., Essery, R., Barr, A., Bartlett, P., Derry, J., Dumont, M., Fierz, C., Kim, H., Kontu, A., Lejeune, Y., Marks, D., Niwano, M., Raleigh, M., Wang, L., and Wever, N.: Meteorological and evaluation datasets for snow modelling at 10 reference sites: description of in situ and bias-corrected reanalysis data, *Earth Syst. Sci. Data*, 11, 865–880, <https://doi.org/10.5194/essd-11-865-2019>, 2019.
- 850 Menard, C. B., Essery, R., Krinner, G., Arduini, G., Bartlett, P., Boone, A., Brutel-Vuilmet, C., Burke, E., Cuntz, M., Dai, Y., Decharme, B., Dutra, E., Fang, X., Fierz, C., Gusev, Y., Hagemann, S., Haverd, V., Kim, H., Lafaysse, M., Marke, T., Nasonova, O., Nitta, T., Niwano, M., Pomeroy, J., Schädler, G., Semenov, V. A., Smirnova, T., Strasser, U., Swenson, S., Turkov, D., Wever, N., and Yuan, H.: Scientific and Human Errors in a Snow Model Intercomparison, *Bulletin of the American Meteorological Society*, 102, E61 – E79, <https://doi.org/10.1175/BAMS-D-19-0329.1>, 2021.



- 855 Minder, J. R., Durran, D. R., and Roe, G. H.: Mesoscale controls on the mountainside snow line, *Journal of the atmospheric sciences*, 68, 2107–2127, 2011.
- Mital, U., Dwivedi, D., Brown, J. B., and Steefel, C. I.: Downscaled hyper-resolution (400m) gridded datasets of daily precipitation and temperature (2008–2019) for the East–Taylor subbasin (western United States), *Earth System Science Data*, 14, 4949–4966, <https://doi.org/10.5194/essd-14-4949-2022>, 2022.
- 860 Monteiro, D., Caillaud, C., Samacoïts, R., Lafaysse, M., and Morin, S.: Potential and limitations of convection-permitting CNRM-AROME climate modelling in the French Alps, *International Journal of Climatology*, 42, 7162–7185, <https://doi.org/https://doi.org/10.1002/joc.7637>, 2022.
- Morin, S., Horton, S., Techel, F., Bavay, M., Coléou, C., Fierz, C., Gobiet, A., Hagenmuller, P., Lafaysse, M., Ližar, M., Mitterer, C., Monti, F., Müller, K., Olefs, M., Snook, J. S., van Herwijnen, A., and Vionnet, V.: Application of physical snowpack models in support of  
865 operational avalanche hazard forecasting: A status report on current implementations and prospects for the future, *Cold Reg. Sci. Tech.*, 170, 102 910, <https://doi.org/10.1016/j.coldregions.2019.102910>, 2020.
- Mott, R., Faure, F., Lehning, M., Löwe, H., Hynek, B., Michlmayer, G., Prokop, A., and Schöner, W.: Simulation of seasonal snow-cover distribution for glacierized sites on Sonnblick, Austria, with the Alpine3D model, *Annals of Glaciology*, 49, 155–160, <https://doi.org/10.3189/172756408787814924>, 2008.
- 870 Mott, R., Schirmer, M., Bavay, M., Grünewald, T., and Lehning, M.: Understanding snow-transport processes shaping the mountain snow-cover, *The Cryosphere*, 4, 545–559, <https://doi.org/10.5194/tc-4-545-2010>, publisher: Copernicus GmbH, 2010.
- Mott, R., Scipión, D., Schneebeli, M., Dawes, N., Berne, A., and Lehning, M.: Orographic effects on snow deposition patterns in mountainous terrain, *Journal of Geophysical Research: Atmospheres*, 119, 1419–1439, <https://doi.org/10.1002/2013JD019880>, 2014.
- Mott, R., Vionnet, V., and Grünewald, T.: The Seasonal Snow Cover Dynamics: Review on Wind-Driven Coupling Processes, *Front. Earth Sci.*, 6, 197, <https://doi.org/10.3389/feart.2018.00197>, 2018.
- 875 Mott, R., Winstral, A., Cluzet, B., Helbig, N., Magnusson, J., Mazzotti, G., Quéno, L., Schirmer, M., Webster, C., and Jonas, T.: Operational snow-hydrological modeling for Switzerland, *Frontiers in Earth Science*, 11, 1228 158, 2023.
- Musselman, K. N., Pomeroy, J. W., Essery, R. L., and Leroux, N.: Impact of windflow calculations on simulations of alpine snow accumulation, redistribution and ablation, *Hydrological Processes*, 29, 3983–3999, 2015.
- 880 Nachtergaele, F., Velthuisen, H., Verelst, L., and Wiberg, D.: Harmonized world soil database (hwsd), Food and Agriculture Organization of the United Nations, Rome, 2009.
- Pepin, N., Bradley, R. S., Diaz, H. F., Baraer, M., Caceres, E. B., Forsythe, N., Fowler, H., Greenwood, G., Hashmi, M. Z., Liu, X. D., Miller, J. R., Ning, L., Ohmura, A., Palazzi, E., Rangwala, I., Schöner, W., Severskiy, I., Shahgedanova, M., Wang, M. B., Williamson, S. N., Yang, D. Q., and Mountain Research Initiative EDW Working Group: Elevation-dependent warming in mountain regions of the world,  
885 *Nature Climate Change*, 5, 424–430, <https://doi.org/10.1038/nclimate2563>, number: 5 Publisher: Nature Publishing Group, 2015.
- Pomeroy, MacDonald, M., DeBeer, C., and Brown, T.: Modeling Alpine Snow Hydrology in the Canadian Rocky Mountains, <https://westernsnowconference.org/node/747>, 2009.
- Pomeroy, J. and Gray, D.: Snow accumulation, relocation and management, Tech. Rep. 7, National Hydrology Research Institute Science. Environnement Canada, 1995.
- 890 Pomeroy, J., Gray, D., Shook, K., Toth, B., Essery, R., Pietroniro, A., and Hedstrom, N.: An evaluation of snow accumulation and ablation processes for land surface modelling, *Hydrological Processes*, 12, 2339–2367, 1998.



- Prasad, R., Tarboton, D. G., Liston, G. E., Luce, C. H., and Seyfried, M. S.: Testing a blowing snow model against distributed snow measurements at Upper Sheep Creek, Idaho, United States of America, *Water Resources Research*, 37, 1341–1356, <https://doi.org/10.1029/2000WR900317>, 2001.
- 895 Quéno, L., Karbou, F., Vionnet, V., and Dombrowski-Etchevers, I.: Satellite-derived products of solar and longwave irradiances used for snowpack modelling in mountainous terrain, *Hydrology and Earth System Sciences*, 24, 2083–2104, 2020.
- Quéno, L., Vionnet, V., Dombrowski-Etchevers, I., Lafaysse, M., Dumont, M., and Karbou, F.: Snowpack modelling in the Pyrenees driven by kilometric-resolution meteorological forecasts, *The Cryosphere*, 10, 1571–1589, <https://doi.org/10.5194/tc-10-1571-2016>, 2016.
- Quéno, L., Mott, R., Morin, P., Cluzet, B., Mazzotti, G., and Jonas, T.: Snow redistribution in an intermediate-complexity snow hydrology  
900 modelling framework, *EGUsphere*, p. 1–32, <https://doi.org/10.5194/egusphere-2023-2071>, 2023.
- Raleigh, M. S., Lundquist, J. D., and Clark, M. P.: Exploring the impact of forcing error characteristics on physically based snow simulations within a global sensitivity analysis framework, *Hydrol. Earth Syst. Sci.*, 19, 3153–3179, <https://doi.org/10.5194/hess-19-3153-2015>, 2015.
- Revuelto, J., Lecourt, G., Lafaysse, M., Zin, I., Charrois, L., Vionnet, V., Dumont, M., Rabatel, A., Six, D., Condom, T., et al.: Multi-Criteria Evaluation of Snowpack Simulations in Complex Alpine Terrain Using Satellite and In Situ Observations, *Remote Sens.*, 10,  
905 1171, <https://doi.org/10.3390/rs10081171>, 2018.
- RGI Consortium: Randolph Glacier inventory—a dataset of global glacier outlines: Version 6.0, <https://doi.org/https://doi.org/10.7265/4m1f-gd79>, 2017.
- Rüschendorf, L.: The Wasserstein distance and approximation theorems, *Probability Theory and Related Fields*, 70, 117–129, <https://doi.org/10.1007/BF00532240>, 1985.
- 910 Sato, T., Kimura, T., Ishimaru, T., and Maruyama, T.: Field test of a new snow-particle counter (SPC) system, *Annals of Glaciology*, 18, 149–154, <https://doi.org/10.3189/S0260305500011411>, 1993.
- Schirmer, M. and Jamieson, B.: Verification of analysed and forecasted winter precipitation in complex terrain, *The Cryosphere*, 9, 587–601, <https://doi.org/10.5194/tc-9-587-2015>, 2015.
- Schlögl, S., Marty, C., Bavay, M., and Lehning, M.: Sensitivity of Alpine3D modeled snow cover to modifications in  
915 DEM resolution, station coverage and meteorological input quantities, *Environmental Modelling & Software*, 83, 387–396, <https://doi.org/10.1016/j.envsoft.2016.02.017>, 2016.
- Schneiderbauer, S. and Prokop, A.: The atmospheric snow-transport model: SnowDrift3D, *Journal of Glaciology*, 57, 526–542, <https://doi.org/10.3189/002214311796905677>, 2011.
- Seity, Y., Brousseau, P., Malardel, S., Hello, G., Bénard, P., Bouttier, F., Lac, C., and Masson, V.: The AROME-France convective scale  
920 operational model, *Mon. Weather Rev.*, 129, 976–991, 2011.
- Sen Gupta, A. and Tarboton, D. G.: A tool for downscaling weather data from large-grid reanalysis products to finer spatial scales for distributed hydrological applications, *Environmental Modelling & Software*, 84, 50–69, <https://doi.org/10.1016/j.envsoft.2016.06.014>, 2016.
- Sharma, V., Gerber, F., and Lehning, M.: Introducing CRYOWRF v1.0: Multiscale atmospheric flow simulations with advanced snow cover  
925 modelling, *Geoscientific Model Development Discussions*, 2021, 1–46, <https://doi.org/10.5194/gmd-2021-231>, 2021.
- Strasser, U., Bernhardt, M., Weber, M., Liston, G., and Mauser, W.: Is snow sublimation important in the alpine water balance?, *The Cryosphere*, 2, 53–66, 2008.
- Tong, J., Déry, S., and Jackson, P.: Topographic control of snow distribution in an alpine watershed of western Canada inferred from spatially-filtered MODIS snow products, *Hydrology and Earth System Sciences*, 13, 319–326, 2009.



- 930 Vernay, M., Lafaysse, M., Monteiro, D., Hagenmuller, P., Nheili, R., Samacoits, R., Verfaillie, D., and Morin, S.: The S2M meteorological and snow cover reanalysis over the French mountainous areas: description and evaluation (1958–2021), *Earth System Science Data*, 14, 1707–1733, <https://doi.org/10.5194/essd-14-1707-2022>, 2022.
- Vionnet, V., Brun, E., Morin, S., Boone, A., Martin, E., Faroux, S., Le-Moigne, P., and Willemet, J.-M.: The detailed snowpack scheme Crocus and its implementation in SURFEX v7.2, *Geosci. Model. Dev.*, 5, 773–791, <https://doi.org/10.5194/gmd-5-773-2012>, 2012.
- 935 Vionnet, V., Martin, E., Masson, V., Guyomarc’h, G., Naaim-Bouvet, F., Prokop, A., Durand, Y., and Lac, C.: Simulation of wind-induced snow transport and sublimation in alpine terrain using a fully coupled snowpack/atmosphere model, *The Cryosphere*, 8, 395–415, <https://doi.org/10.5194/tc-8-395-2014>, 2014.
- Vionnet, V., Martin, E., Masson, V., Lac, C., Naaim Bouvet, F., and Guyomarc’h, G.: High-Resolution Large Eddy Simulation of Snow Accumulation in Alpine Terrain, *J. Geophys. Res. Atmos.*, 122, 11,005–11,021, <https://doi.org/10.1002/2017JD026947>, 2017.
- 940 Vionnet, V., Six, D., Auger, L., Dumont, M., Lafaysse, M., Quéno, L., Réveillet, M., Dombrowski Etchevers, I., Thibert, E., and Vincent, C.: Sub-kilometer precipitation datasets for snowpack and glacier modeling in alpine terrain, *Front. Earth Sci.*, 7, 182, <https://doi.org/10.3389/feart.2019.00182>, 2019.
- Vionnet, V., Marsh, C. B., Menounos, B., Gascoin, S., Wayand, N. E., Shea, J., Mukherjee, K., and Pomeroy, J. W.: Multi-scale snowdrift-permitting modelling of mountain snowpack, *The Cryosphere*, 15, 743–769, <https://doi.org/10.5194/tc-15-743-2021>, 2021.
- 945 Vionnet, V., Verville, M., Fortin, V., Brugman, M., Abrahamowicz, M., Lemay, F., Thériault, J. M., Lafaysse, M., and Milbrandt, J. A.: Snow Level From Post-Processing of Atmospheric Model Improves Snowfall Estimate and Snowpack Prediction in Mountains, *Water Resour. Res.*, 58, e2021WR031778, <https://doi.org/10.1029/2021WR031778>, 2022.
- Vionnet, V., Dombrowski-Etchevers, I., Lafaysse, M., Quéno, L., Seity, Y., and Bazile, E.: Numerical weather forecasts at kilometer scale in the French Alps : evaluation and applications for snowpack modelling, *J. Hydrometeor.*, <https://doi.org/10.1175/JHM-D-15-0241.1>, 2016.
- 950 Wang, Z. and Huang, N.: Numerical simulation of the falling snow deposition over complex terrain, *Journal of Geophysical Research: Atmospheres*, 122, 980–1000, <https://doi.org/10.1002/2016JD025316>, eprint: <https://onlinelibrary.wiley.com/doi/pdf/10.1002/2016JD025316>, 2017.
- Whitebox Geospatial: WhiteboxTools open core, Whitebox Geospatial Inc, [https://www.whiteboxgeo.com/manual/wbt\\_book/available\\_tools/geomorphometric\\_analysis.html#Geomorphons](https://www.whiteboxgeo.com/manual/wbt_book/available_tools/geomorphometric_analysis.html#Geomorphons), 2023.
- 955 Whiteman, C. D.: *Mountain meteorology: fundamentals and applications*, Oxford University Press, 2000.
- Winstral, A., Elder, K., and Davis, R. E.: Spatial snow modeling of wind-redistributed snow using terrain-based parameters, *Journal of hydrometeorology*, 3, 524–538, 2002.
- Yang, J., Yau, M., Fang, X., and Pomeroy, J.: A triple-moment blowing snow-atmospheric model and its application in computing the seasonal wintertime snow mass budget, *Hydrol. Earth Sys. Sci.*, 14, 1063–1079, <https://doi.org/10.5194/hess-14-1063-2010>, 2010.
- 960 Yu, N., Gaussiat, N., and Tabary, P.: Polarimetric X-band weather radars for quantitative precipitation estimation in mountainous regions, *Quarterly Journal of the Royal Meteorological Society*, 144, 2603–2619, <https://doi.org/10.1002/qj.3366>, 2018.